A Section 508–conformant HTML version of this article is available at https://doi.org/10.1289/EHP14426.

Integrated Studies on Male Reproductive Toxicity of Decabromodiphenyl Ethane in Zebrafish Spermatozoa *Ex Vivo*, Male Zebrafish *in Vivo*, and GC-1 Cells *in Vitro*

Lihua Yang,[1] Yindan Zhang,[1,2]* Jianghuan Hua,[1,3,4] Guili Song,[1] Fan Li,[1,2] Na Zheng,[1,2] Taotao Zhang,[3] Zhixiang Xu,[1,5] Xinxin Ren,[1,2] Biran Zhu,[1,3] Yanna Han,[6] Yongyong Guo,[1] Jian Han,[1] and Bingsheng Zhou[1]*

[1]Key Laboratory of Breeding Biotechnology and Sustainable Aquaculture, Institute of Hydrobiology, Chinese Academy of Sciences, Wuhan, People's Republic of China
[2]University of Chinese Academy of Sciences, Beijing, People's Republic of China
[3]School of Basic Medical Sciences, Hubei University of Chinese Medicine, Wuhan, People's Republic of China
[4]Hubei Shizhen Laboratory, Wuhan, People's Republic of China
[5]College of Fisheries and Life Science, Dalian Ocean University, Dalian, People's Republic of China
[6]Key Laboratory of Environmental Risk Assessment and Control on Chemical Process, School of Resource and Environmental Engineering, East China University of Science and Technology, Shanghai, People's Republic of China

Background: Legacy brominated flame retardants have been recognized as risky factors leading to declined sperm quality. The widespread utilization of decabromodiphenyl ethane (DBDPE) as a replacement for decabromodiphenyl ether has given rise to considerable concern over its potential risks to reproductive health.

Objectives: The objectives were to quickly determine whether DBDPE affects sperm quality upon *ex vivo* exposure, to reveal the reproductive outcomes and underlying molecular mechanisms using an *in vivo* zebrafish model exposed to DBDPE, and to validate the potential impact on DNA damage and energy metabolism balance *in vitro*.

Methods: Zebrafish spermatozoa were treated with DBDPE (0.01, 0.1, 1, 10 μM) for 3 h, and the spermatozoa motility and fertilization ability with normal eggs were evaluated. Then adult male zebrafish were treated with DBDPE (0.1, 1, 10, and 100 nM) for 2 months, and their reproductive performance was examined. Four-dimensional label-free proteome and phosphoproteome were performed in zebrafish testes, and the findings were validated by multiple indicators. Finally, mouse spermatogonial GC-1 cells were treated with DBDPE (0.1, 1 μM) for 72 h, and DNA damage was examined, as well as the energy production of glycolysis and oxidative phosphorylation.

Results: *Ex vivo* exposure to DBDPE caused lower motility and fertilization rates of zebrafish spermatozoa. *In vivo* exposure to DBDPE caused lower sperm motility and abnormal spermatogenesis in male zebrafish testes. Integrated whole-proteome and phosphoproteome analysis revealed DNA damage responses and energy metabolic disorders in zebrafish testes. A dosage window characterized by higher mitochondrial membrane potential (MMP) in combination with unchanged reactive oxygen species and apoptosis rates was observed in both zebrafish testes and GC-1 cells.

Discussion: This study suggests that in zebrafish, DBDPE exposure could impair sperm quality and spermatogenesis, and the underlying mechanism could be related to DNA damage and energy metabolic reprogramming in testicular germ cells. https://doi.org/10.1289/EHP14426

Introduction

In recent decades, declining male reproductive capacity has become a global concern, with decreasing semen quality and quantity evident.[1,2] Extensive evidence implicates environmental pollution rather than genetic factors as the leading risk factor for male reproductive health of various organisms.[3,4] Among the growing list of pollutants, some brominated flame retardants (BFRs) are both persistent organic pollutants and endocrine-disrupting chemicals (EDCs) and have been repeatedly associated with declining sperm quality in both epidemiological and laboratory investigations.[5,6] Governments have restricted the application of some BFRs in various plastics, as well as in electronic and textile products, and replacement chemicals are needed to ensure that products meet safety standards.[7,8]

Typically, decabromodiphenyl ethane (DBDPE) has been employed as an alternative to decabromodiphenyl ether (BDE209) since the 1990s. In a recent study in China, the major producer and exporter of BFRs,[9,10] BDE209 and DBDPE were identified as the most predominant BFRs in the agricultural soils from different regions, and the DBDPE concentration increased rapidly between 2011 and 2021, with a doubling time of 6.84 y.[11] In surface waters, the detected concentrations of DBDPE typically hover in the picograms-per-liter range, sometimes reaching the range of several to several tens of nanograms per liter,[12–14] and occasionally reaching 107 ng/L.[15] Concentrations of DBDPE were detected at a concentration of up to 80 ng/L in seepage water from a metal recycling site in Norway[16] and up to 990 ng/L in sewage outlets along the Dongjinang River in China.[17] Furthermore, DBDPE has been widely detected in aquatic organisms worldwide,[18,19] and the measured mean concentrations of DBDPE were 1,700 ± 744 ng/g lipid weight (lw) and 11,800 ± 4,400 ng/g lw in crucian carp (*Carassius auratus*) and tilapia (*Oreochromis* spp.) at an e-waste recycling site in South China.[20] Notably, DBDPE tends to bioaccumulate at higher levels in humans living in more severely contaminated areas. It has been detected in serum and milk samples from nonoccupational populations living in BFR-producing areas[21,22] and general city populations from no-novel-brominated-flame-retardant (NBFR)-producing areas.[23–25] Serum levels of DBDPE in nonoccupational populations (detection frequency 98%) from a BFR-producing area were up to 6,660 ng/L (1,590 ng/g lw), with a median concentration of 153 ng/L (32.5 ng/glw).[22] Therefore, DBDPE is considered a major

*These authors contributed equally to this work.

Address correspondence to Jianghuan Hua, School of Basic Medical Sciences, Hubei University of Chinese Medicine, Wuhan People's Republic of China. Email: huajianghuan@163.com. And, Bingsheng Zhou, Institute of Hydrobiology, Chinese Academy of Sciences, Donghu South Rd., Wuchang District, Wuhan 430072, the People's Republic of China. Email: bszhou@ihb.ac.cn

Supplemental Material is available online (https://doi.org/10.1289/EHP14426).

The authors declare they have nothing to disclose.

Conclusions and opinions are those of the individual authors and do not necessarily reflect the policies or views of EHP Publishing or the National Institute of Environmental Health Sciences.

Received 6 December 2023; Revised 6 September 2024; Accepted 24 October 2024; Published 21 November 2024.

Note to readers with disabilities: *EHP* strives to ensure that all journal content is accessible to all readers. However, some figures and Supplemental Material published in *EHP* articles may not conform to 508 standards due to the complexity of the information being presented. If you need assistance accessing journal content, please contact ehpsubmissions@niehs.nih.gov. Our staff will work with you to assess and meet your accessibility needs within 3 working days.

BFR pollutant, and it may pose an increasing exposure risk to humans, as well as to domestic and wild animals, not only in China, but also across the globe.[26–28]

Paradoxically, to ensure good flame retardancy, alternatives usually share similar molecular structures with these legacy chemicals, thereby exhibiting similar chemical properties, environmental behavior, and even biological toxicity. This has resulted in widespread doubt about the safety of substitute BFRs.[29] Typically, DBDPE persists in the environment, accumulates in organisms, and has been associated with thyroid disruption and neurotoxicity *in vitro*[30] and *in vivo* (in nemotodes[31] and zebrafish[32]), and these are typical features of BDE209.[33,34] Researchers have reported fewer sperm, with diminished motility, in male rats following oral administration with DBDPE at 50 or 500 mg/kg per day, followed by DNA damage and apoptosis in testes.[35–37] Our recent studies found that DBDPE exhibited typical characteristics of endocrine metabolism-disrupting chemicals (also called metabolic EDCS), which can demonstrate endocrine-disrupting effects and the capacity to affect cellular energy metabolism.[37–39] Therefore, a more complicated underlying mechanism may contributed to DBDPE-induced toxic effects, given that these two processes are intricately interconnected.[39,40] However, our current knowledge of the adverse impacts of DBDPE is far from adequate for properly assessing its potential risks to humans and animals. For one thing, the exposure doses in the abovementioned studies were much higher than the exposure levels in wild animals and humans. Furthermore, it is urgent to know whether DBDPE can have adverse effects on male reproduction at environmentally relevant concentrations. In addition, testes show some specificity because spermatogenic cells mainly use lactate as their energy substrate,[41] a phenomenon that is similar to the Warburg effects reported in various cancer cells.[42] Researchers have identified a variety of cancer/testis antigens that are specifically involved in the metabolic shift during spermatogenesis and tumorigenesis,[43] which may pose more challenges in revealing the potential mechanism of male reproductive toxicity. Therefore, probing the responsive mechanisms in testes upon DBDPE exposure at environmentally relevant concentrations is a priority for properly assessing its environmental health risks.

Moreover, to keep pace with the rapidly increasing number of emerging pollutants, exploring new approach methodologies (NAMs) to expedite risk assessment has attracted global attention.[39] High-throughput omics methods can provide comprehensive knowledge of the biological status at the molecular level in response to pollutants, and such approaches have been widely used to assess the toxic effects of new pollutants.[44,45] The zebrafish is a valuable model for developing NAMs to investigate endocrine and metabolic disruption, allowing extrapolation to potential effects on wild fish and even human health.[39] Researchers have also established spermatozoa exposure protocols that take advantage of external fertilization in fish.[46,47] In this regard, DBDPE could be an appropriate example for exploring NAMs comprising *in vitro*, *ex vivo*, and non-rodent *in vivo* tests for future pollutant risk assessment. Thus, this study aimed to *a*) rapidly screen the potential effects of DBDPE on sperm using *ex vivo* exposure of zebrafish spermatozoa followed by artificial fertilization, *b*) evaluate whether DBDPE could impair spermatozoa quality and spermatogenesis in zebrafish following *in vivo* exposure, *c*) reveal the molecular responsive profiles in zebrafish testes using an integrated proteome and phosphoproteome approach, and *d*) validate the potential impact on DNA damage and energy metabolism balance using *in vitro* cells. The results not only expand our understanding of the toxic mechanisms of DBDPE but could also facilitate the development of NAMs in future studies.

Materials and Methods

Chemicals and Reagents

DBDPE [Chemical Abstracts Service (CAS): 84852-53-9; purity >96%] for fish exposure was obtained from Tokyo Chemical Industry Co. Ltd. Standards for chemical analysis, including DBDPE (≥99%) and isotope-labeled $^{13}C_{12}$-BDE-209 (CAS: 562099-68-7; purity ≥99%), were supplied by AccuStandard Inc. Dimethyl sulfoxide (DMSO; CAS: 67-68-5; purity >99.9%), methanesulfonate (MS-222), and lactate dehydrogenase (LDH) inhibitor oxamic acid (oxamate) were obtained from Sigma-Aldrich. Dulbecco's Modified Eagle medium (DMEM) and fetal bovine serum (FBS) for cell culture were supplied by Shanghai VivaCell Biosciences Ltd. Penicillin and streptomycin were provided by Beijing Solarbio Science & Technology Co. Ltd. All other reagents used in this study were of chromatography or analytical grade.

Zebrafish Maintenance and Exposure

Wild-type zebrafish (AB strain) used in the present study were obtained from the China Zebrafish Resource Center of the National Aquatic Biological Resource Center (CZRC-NABRC). Six-month-old healthy male zebrafish were randomly selected and placed into glass tanks (20 fish/tank) containing 20 L of charcoal-filtered tap water with pH 7.0–7.4 and maintained at 28 ± 0.5°C under a 14:10 light/dark cycle. The fish were fed fresh fairy shrimp twice a day. The care and use of zebrafish was performed under the approval of the institutional animal care and use committee of the Institute of Aquatic Biology, Chinese Academy of Sciences.

Measurement of Spermatozoa Motility in Ex Vivo *Test*

Zebrafish spermatozoa have been used as a good toxicological test system because of their simplicity and availability, and their motility changes can be used to predict reproductive success as an ecologically relevant effect.[48,49] In this study, *ex vivo* zebrafish spermatozoa exposure was first performed to rapidly screen the potential effects of DBDPE on sperm. Ten unexposed male zebrafish (AB strain; 8 months old) were anesthetized with 150 mg/L of MS-222[50] and dried with paper towels, and their abdomens were gently massaged with fingers to release semen from the zebrafish cloaca. The semen samples were collected and pooled into a centrifuge tube containing Hanks' balanced salt solution (HBSS; 300 mOsmol/kg), a solution in which zebrafish spermatozoa can stay in static status. Then the fish were placed into water to recover within 3–5 min.[50] A total of 70 males were used to collect fresh semen, and seven tubes of fresh semen samples were obtained. Then the seven tubes of semen samples were divided into 14 samples ($n = 14$). The spermatozoa concentrations were estimated using a cell counting chamber (Marienfeld Superior) and adjusted to ensure equal concentrations among all samples at 5×10^8 spermatozoa/mL. In general, zebrafish spermatozoa can be maintained in a healthy state in HBSS for 6 h when stored at 0–4°C. To determine exposure concentrations and durations in the formal experiment, we performed an incubated exposure experiment.[48,49] In the incubated exposure experiment, spermatozoa suspension was first incubated in HBSS containing a series of DBDPE concentrations (0.01, 0.1, 1, 10 μM) for 3 or 6 h on ice, with subsequent analysis of sperm motility (detailed methods are described below).

Based on the results of the pre-experiment, we finally exposed zebrafish spermatozoa to a series of DBDPE concentrations (0.01, 0.1, 1, 10 μM) for 3 h on ice. The lowest concentration (0.01 μM = 9,710 ng/L) of DBDPE was on the same order of magnitude as the highest concentration (6,660 ng/L) detected in

the serum samples from the nonoccupational population from a BFR-producing area.[22] A blank control (HBSS) and a solvent control (DMSO) were also included. The solvent control and all DBDPE treatments received 0.05% DMSO. To minimize errors due to pre-exposure sperm itself (e.g., status of males), semen samples in different treatments were from the same batches of male zebrafish. The detailed protocol and procedures for preparing the exposure solution and the exposure system are as follows: DBDPE was first dissolved in DMSO to configure a 20,000 μM DBDPE stock solution, which was then diluted in a gradient with DMSO to obtain a series of DBDPE working solutions with concentrations of 20,000, 2,000, 200, and 20 μM. One microliter of DMSO or DBDPE working solution was added to 1,000 μL of HBSS to configure a 2× exposure solution, to be used within 1 d. Five microliters of each well-prepared semen sample in HBSS and 5 μL of the 2× exposure solution were mixed in a tube at 4°C to obtain the exposure system, and the final concentrations contained $\sim 2.5 \times 10^8$ sperm/mL.

After 3 h of exposure, each spermatozoa suspension sample was used for sperm motility analysis. Briefly, 1 μL of spermatozoa suspension was placed on a slide (Hamilton Thorne; #223120), which was placed on a CX41 microscope (Olympus), and 1 μL of deionized water was added and mixed quickly to activate the spermatozoa (induction of spermatozoa movement due to osmoticity changes), followed by the addition of a coverslip. Then six sperm motility parameters (see Table S1 for definitions), including *a*) total motility (TM; in percentage), *b*) progressive motility (PM; in percentage), *c*) average path velocity (VAP; in micrometers per second), *d*) velocity of spermatozoa linear motion (VSL; in micrometers per second), *e*) velocity of sperm (VCL; in micrometers per second), and *f*) sperm linearity (LIN; in percentage) were immediately measured using an IVOS Sperm Analyzer (Hamilton Thorne) and HT CASA II Animal Motility Software (version 1.8; Hamilton Thorne).[51] The computer-assisted sperm analysis (CASA) input parameters used in this study are shown in Table S2, with slight modifications based on previous studies.[19,48] A minimum of 300 sperm cells were tracked per field, at least three fields captured for each sample, and each sample was measured at least twice.

Measurement of Offspring Development in Ex Vivo *Test*

Fresh semen samples ($n = 3$/group) exposed for 3 h in the same way and with the same doses as described above were used for artificial fertilization with eggs from unexposed female zebrafish (AB strain; 8-month-old), according to a previously described method.[51] Briefly, on the day before egg collection, unexposed females were isolated from the males (AB strain; 8-month-old). Egg collection and artificial fertilization were performed at the end of sperm exposure in the morning. Before egg stripping, four females were fully anesthetized with MS-222 and gently dried with paper towels, and their abdomens were gently massaged with fingers to collect unfertilized eggs into a Petri dish. Pooled eggs from four fish were mixed gently, then evenly divided into six 35-mm Petri dishes (corresponding to 6 exposed groups) as quickly as possible, and semen samples exposed to DBDPE for 3 h (another subset of exposed semen samples from the above-mentioned *ex vivo* zebrafish spermatozoa exposure experiment) were added to the six Petri dishes containing the eggs. The ratio of eggs to spermatozoa was $\sim$150–200: 2.5×10^6. A 750-μL volume of charcoal-filtered tap water (pH 7.0–7.4) was added to each Petri dish and blown evenly with a straw to activate the sperm, ensuring full contact with eggs. After incubating at room temperature for 5 min, the fertilized eggs in each Petri dish were washed three times with charcoal-filtered tap water and transferred to 90-mm Petri dishes to remove possible residual DBDPE. The obtained embryos were then cultured at 28 ± 0.5°C under a 14:10 light/dark cycle until 120 h post-hatching (hpf).

The embryos were observed under a SMZ745T dissecting microscope (Nikon). Unfertilized eggs were distinguished at about 3 h by phenotypes of whiteness, opacity, and failure of embryonic development,[51,52] and the fertilization rate was determined. Four end points were recorded daily as indicators of lethality: *a*) coagulation of embryos, *b*) lack of somite formation, *c*) nondetachment of the tail, and *d*) lack of heartbeat.[52] Malformation phenotypes were observed daily, including, for example, yolk sac edema, pericardial edema, uninflated swim bladder, and spinal scoliosis.[53] The survival rate was determined at 24, 48, and 120 hpf, and the malformation rate was determined at 120 hpf. All these development indicators of zebrafish offspring were repeated three times.

In Vivo *Exposure*

After 2 wk of acclimatization, adult male fish (6-month-old) were exposed to a series of DBDPE concentrations (0, 0.1, 1, 10, 100 nM; corresponding to 0, 97.1, 971.2, 9,712.0, 97,120.4 ng/L) for 2 months. This exposure window was chosen taking into account the fact that male zebrafish exhibit their peak reproductive capacity during the age of 6 to 8 months. The selected exposure concentrations included an environmentally relevant concentration (0.1 nM = 97.1 ng/L) in surface waters, where DBDPE was detected, with concentrations at several to several tens of nanograms per liter and as high as 107 ng/L.[12,14,15] There were three replicate tanks for each exposure group, and the exposure solution was 100% renewed daily. At the end of exposure, 21 fish from each group were randomly chosen for subsequent measurement of reproductive behavior. Then, all the fish were euthanized with 300 mg/L of MS-222, body length and body weight were measured, and condition factors were calculated [wet body weight (in grams)/total body length $(\text{in centimeters})^3 \times 100\%$]. The testes were isolated, weighed, and then stored at −80°C for subsequent analysis.

Cell Culture and Treatment

The *in vitro* test was performed to verify the observations of DNA damage and energy reprogramming in zebrafish testes upon DBDPE exposure. Mouse spermatogonial GC-1 cells purchased from FuHeng Cell Center were cultured in DMEM with 10% FBS, 100 IU/mL of penicillin, and 0.1 mg/mL of streptomycin, and incubated at 37°C in a humidified 5% carbon dioxide (CO_2)/95% air incubator. Cells were seeded in 96-well (20,000 cells/well) or 6-well (400,000 cells/well) plates overnight to adhere, then treated with a series of concentrations of DBDPE (0.1 and 1 μM) and the LDH inhibitor oxamic acid (oxamate; 20 mM)[54] for 72 h. Before this formal experiment, we performed a pre-experiment by exposing GC-1 cells to a series of concentrations of DBDPE (0.01, 0.1, 1, 10 μM) for 48 h to investigate its effects on MMP and adenosine triphosphate (ATP) content. The exposure concentrations and duration of DBDPE used in the formal experiment were set based on our pre-experiment (results are shown in the "Results" section). A 20 M oxamate stock solution was prepared with water, stored at −80°C, to be used within 7 d. All the treatment groups and the control group received 0.1% DMSO.

Reproductive Behavior and Offspring Development in Zebrafish

At the end of the exposure, 21 exposed male zebrafish from each group were randomly selected and paired with unexposed females for reproductive behavior tests according to a previously described method.[55] One exposed male and one unexposed female were placed into a tank (length: 22.6 cm, width:

11.3 cm, height: 11.2 cm) and separated by a divider overnight. The next morning between 08:00 and 09:00, the divider was removed when the lights were turned on, and reproductive behavior was monitored for 30 min using an FDR-AX60 video camera (Sony) mounted above the tank. The obtained videos were imported into EthoVision XT 14 video tracking software (Noldus Inc.) and mating-related parameters of zebrafish reproductive behavior, including proximity, proximity frequency, body contact, body contact frequency, and body contact cumulative duration, were analyzed. Mating behavior was defined as a distance of no more than 1.5 cm between male and female fish and sustained movement for >5 s. After behavior assessment, the resulting eggs were collected immediately in clean water, transferred into clean charcoal-filtered tap water, and cultured in an incubator at $28 \pm 0.5^{\circ}C$ under a 14:10 light/dark cycle. The fertilization rate, hatching rate at 72 hpf, and both malformation rate and survival rate at 120 hpf were determined as described above.

Quantification of DBDPE Contents in Zebrafish Testes

Testes from three exposed zebrafish from the same replicate tank were pooled as one replicate sample ($n = 3$ replicates), and DBDPE contents were determined according to our previous method.[32] After freeze-drying, each testes sample was spiked with $^{13}C_{12}$-BDE209 as the internal standard and then homogenized with 5 mL of *n*-hexane. After ultrasound sonication for 60 min, all samples were centrifuged at 2,000 rpm ($733 \times g$) for 10 min, and the supernatants were subsequently collected. The samples were extracted once more with 5 mL of *n*-hexane, and the supernatants from two extractions were combined. The supernatant was blown dry under nitrogen gas, and the lipid content was determined by gravimetric analysis. The extracts were fully redissolved in 6 mL of *n*-hexane, and 1 mL of concentrated sulfuric acid was added to remove the lipid. After being thoroughly vortexed and allowed to stand for 2 h, the supernatants were subsequently collected and extracted once more with 5 mL of *n*-hexane. The supernatants were combined and further purified by passing them through a multilayered silica column that was packed with neutral silica, acid silica, and anhydrous sodium sulfate, arranged from the bottom to the top. The purified samples were then eluted with *n*-hexane. The effluent was collected, nitrogen dried, and reconstituted in 100 μL of methylbenzene. Then the samples were analyzed and quantified with an Agilent 7890A-5975C gas chromatograph–mass spectrometer (GC–MS) using the electron-capture negative ionization mode in the selected ion monitoring mode, employing a DB-5HT capillary column (15 m length, 0.250 mm diameter, 0.10 μm thickness; J&W Scientific). The column flow rate was 1.8 mL/min. A pulsed non-shunt injection was used with an injection volume of 1 μL. The injection temperature, interface temperature, ion source, and quadrupole were set at 280°C, 320°C, 150°C, and 150°C, respectively. For DBDPE quantification, oven temperature was programmed to hold at 100°C for 1 min before ramping at 30°C/min to 320°C and holding for 3.7 min. Helium (99.999%) was used as the carrier gas, with a constant flow rate of 1.8 mL/min, and methane (99.999%) was used as the reaction gas. Ion fragments *m/z* 79 and 81, *m/z* 494.7 and 496.7 were monitored for DBDPE and $^{13}C_{12}$-BDE209, respectively. The limit of detection (LOD) and limit of quantitation of were 10 and 15 ng/g, respectively. The mean recovery of surrogate $^{13}C_{12}$-BDE209 in the samples was $86\% \pm 3\%$. The recovery of spiked DBDPE was between 82% and 118%.

Spermatozoa Motility and Ultrastructure in In Vivo *Test*

Ten semen samples (each collected from one individual fish; 1 μL of semen per fish) in each group were collected and diluted with HBSS (300 mOsmol/kg) for measurement of spermatozoa motility, as described above. The ultrastructure of spermatozoa was observed by scanning electron microscopy, as previously described.[56] First, 10 μL of fresh semen was collected from at least 10 fish in each group and fixed with 1 mL of 2% glutaraldehyde overnight. After centrifugation ($350 \times g$, 5 min), sperm cells were diluted to 10×10^6 cells/mL with phosphate-buffered saline (PBS) and stored at 4°C. Each spermatozoa sample (5 μL) was gradually dehydrated with ethanol and dried with CO_2 gas on a glass coverslip. The coverslips were glued and gold sputtered, then examined under an S3000 N scanning electron microscopy instrument (Hitachi Ltd.). Approximately 100 random zebrafish spermatozoa scanning electron microscopy micrographs were captured. Images were analyzed using Image-Pro Plus software (version 6.0; https://mediacy.com/image-pro/) to determine the head length, head width, and tail length of the zebrafish spermatozoa.

Gonadal Histological Analysis in Zebrafish

After being anesthetized with 300 mg/L of MS-222 until gill movements had slowed,[56] intact testicular tissues were isolated and weighed to calculate the gonado–somatic index [GSI = gonad weight (in grams)/body weight (in grams) × 100%]. Testes ($n = 9$ fish/group; 3 fish from each replicate tank) were fixed in 4% Paraformaldehyde Fix Solution (PFA) overnight at 4°C, then dehydrated, paraffin-embedded, and sectioned into 4-μm sections. Three tissue sections per fish were collected. The tissue sections were large enough to allow for equal amounts of space between the leading edge of the tissue and the midline of the gonad. The sections were stained with hematoxylin and eosin (H&E) and photographed under a BX53 microscope (Olympus) at a 400× magnification. A total of six random fields without overlap of each section were photographed and quantified. The relative percentages of testicular germ cells at different stages were quantitated by a blind and experienced pathologist by measuring their areas using Image-Pro Plus software (version 6.0; https://mediacy.com/image-pro/).

Four-Dimensional Label-Free Proteome and Phosphoproteome Analysis in Testes

The whole-proteome and phosphoproteome analyses were performed to find clues for possible mechanisms underlying DBDPE-induced reproductive toxicity. Except for the control, only the highest concentration group was selected, based on the result that the zebrafish from this group showed the most significant differences from control in gonad histopathology and that the findings would be further validated by determining multiple indicators at all the test concentrations. Specifically, total protein from zebrafish testicular tissues pooled from nine fish from the same tank ($n = 3$; 9 fish/replicate) was extracted with a lysis buffer containing 4% sodium dodecyl sulfate (SDS), 100 mM dithiothreitol (DTT), and 100 mM Tris-hydrogen chloride, pH 8.0 (i.e., STD lysis buffer), boiled for 3 min, ultrasonicated for 2 min, and centrifuged at $16{,}000 \times g$ for 20 min at 4°C. Protein concentrations in the supernatants were determined using the bicinchoninic acid (BCA) method (Beyotime; #P0009). Protein (200 μg per sample) digestion was performed with a filter-aided sample preparation method, as previously described.[57] First, the detergent (SDS), DTT, and indole-3-acetic acid (IAA) in UA buffer (8 M urea, 150 mM Tris HCL, pH 8.0) were added to block reduced cysteine. The protein suspension was digested with trypsin (Promega) at a ratio of 50:1 overnight at 37°C, followed by centrifugation ($16{,}000 \times g$ for 15 min) and peptide collection. The peptides were desalted with C18 StageTip, and the concentrations of peptides were determined with OD280 by Nanodrop One spectrometer. Phosphopeptides were enriched from digested protein samples using a High-Select Titanium Dioxide Phosphopeptide

Enrichment kit (Thermo Fisher Scientific). Subsequent proteomic and phosphoproteomic sequencing and analysis were performed by Shanghai Bioprofile Technology.

After protein extraction and digestion, the obtained peptides were analyzed by liquid chromatography–tandem MS (LC-MS/MS) in an Easy nLC 1200 instrument (Thermo Scientific) coupled online to a hybrid trapped ion mobility spectrometry (TIMS) quadrupole time-of-flight mass spectrometer (timsTOF Pro; Bruker Daltonics). The peptides were separated on a C18 reversed-phase column (15 cm long, 75 μm internal diameter, 2 μm; Dr. Maisch GmbH) at a flow rate of 300 nL/min. The mobile phases A and B used in this assay were 0.1% formic acid and 0.1% formic acid/80% acetonitrile, respectively. The percentage of B rose linearly from 2% to 22% within 90 min, then increased to 35% within 10 min, and further increased to 80% within the next 8 min before the last 12 min 80% process. Then, the separated peptides were analyzed on a hybrid TIMS quadrupole timsTOF Pro (Bruker Daltonics). The MS was used in a data-dependent acquisition coupled with parallel accumulation serial fragmentation (DDA-PASEF) mode. The accumulation and ramp times were set to 2 and 100 ms, respectively, and mass spectra were collected in the *m/z* 100–1,700 range in positive electrospray mode. Intensity threshold at 5,000 and ion mobility range were scanned from 0.6 to 1.6 Vs/cm^2. Dynamic exclusion time for precursor ions reaching a target value of 20,000 counts was set at 0.4 min. Quadrupole isolation width ranged from 2 *m/z* for *m/z* ratios <700 to 3 *m/z* for *m/z* ratios >700. Each acquisition cycle of 1.1 s comprised 1 full MS scan and 10 PASEF MS/MS scans. The acquired raw data were searched with MSFragger (version 3.4; https://msfragger.nesvilab.org/). Maximum missed cleavages was set to 2 when searching the database. The mass tolerance of 20 ppm for precursor ions and 20 ppm for fragment ions were defined for database search. Carbamidomethylation of cysteines was defined as fixed modification, whereas acetylation of the protein N-terminal and oxidation of methionine were set as variable modifications for database searching. The database search results were filtered and exported with <1% false discovery rate (FDR) both at peptide-spectrum-matched level and protein level. PeptideProphet and ProteinProphet in Philosopher (version 2.2.0; https://philosopher.nesvilab.org/) were used to filter all phosphosites, peptide-spectrum matches, peptides, and proteins. Label-free quantification was conducted with IonQuant (version 1.1.0; Nesvilab). Site quantitation analysis was performed only for phosphorylation sites confidently localized with a localization probability of >0.75. Protein annotation was performed against the zebrafish database in UniProt [https://www.uniprot.org/taxonomy/7955; release: uniprot-Danio rerio (Zebrafish) (Brachydanio rerio) [7955]-62026-20220504]. Kyoto Encyclopedia of Genes and Genomes (KEGG; https://www.genome.jp/kegg/; release 103.1, 1 September 2022) and Gene Ontology (GO; https://geneontology.org/; release 18:31, 2 July 2018) analyses were performed for interpretation of the sequences. Fisher's exact test was applied to conduct KEGG and GO enrichment analyses, and FDR correction was also conducted for multiple testing. Identification of differentially expressed proteins (DEPs) with $\log_2$ (fold change) was performed using R Studio software (https://posit.co/products/open-source/rstudio/). Proteins with $p < 0.05$ and fold change ratios >1.5 were considered DEPs. Differences in phosphosites between DBDPE treatment and control groups were considered significant at $p < 0.05$ and fold change ratios >2. Protein–protein interaction (PPI) networks were constructed using the STRING database (version 12.0; https://cn.string-db.org/) together with Cytoscape software (version 3.9.1; https://cytoscape.org/).

Quantitative Real-Time Polymerase Chain Reaction Analysis

To see whether the biological pathways proposed by proteome and phosphoproteome in testes of fish exposed to 100 nM DBDPE were also affected at lower concentrations, the transcriptional profiles of a list of candidate genes in those pathways were detected by quantitative real-time polymerase chain reaction (qRT-PCR), as previously described.[38] Testes from three exposed zebrafish from the same replicate tank were pooled as one replicate sample ($n = 3$ replicates; the 100 nM DBDPE-exposed group was excluded owing to insufficient samples), and total RNA was extracted with RNAiso Plus reagent (Takara Bio Inc.; #9109), followed by determination of their quality and concentrations on a Nanodrop 2000 platform (Thermo Fisher Scientific). One microgram of total RNA was used as the template for complementary DNA synthesis using a commercial reverse transcription kit (Yeasen Biotech Co., Ltd.; #11141ES60). qRT-PCR was carried out in a total volume of 10 μL using SYBR Green Master Mix (Yeasen Biotechnology Co., Ltd.; #11201ES08) and analyzed on a CFX384 Touch Real-Time PCR Detection System (Bio-Rad Laboratories, Inc.). The programs used are provided in Excel Table S15. Primer sequences of genes are listed in Table S3. The relative transcriptional levels of target genes were normalized using the $2^{-\Delta\Delta Ct}$ method with the protein-coding gene ribosomal protein L8 (*rpl8*) as the reference gene.

Seahorse Assay

The GC-1 cells were pretreated with DBDPE (0.1 and 1 μM; $n = 4$), oxamate (LDH inhibitor, 20 mM; $n = 3$),[54] and DMSO control (0.1% DMSO; $n = 4$) for 72 h and then seeded into poly L-lysine-coated XF24 cell culture microplates (Agilent; #100777-004) in Seahorse XP RPMI medium at a density of 35,000 cells/well. The culture medium contained 5 mM glucose (Sigma-Aldrich; #G8270-100G), 1 mM sodium pyruvate, and 2 mM L-glutamine (Thermo Fisher Scientific; #25030081). Before detection, the probe plates were hydrated overnight using high-performance LC (HPLC)–grade water and then calibrated with XF Calibrant for at least 1 h at 37°C. The ATP production rates of glycolysis and mitochondrial oxidative phosphorylation were measured using an Agilent Seahorse XF Real-Time ATP Rate Assay Kit (Agilent; #103592–100) and an XFe24 Extracellular Flux Analyzer (Agilent), following the manufacturer's instructions.

Biochemical Measurement

Zebrafish testicular tissues (3 testes from 3 fish pooled as 1 replicate sample) and GC-1 cells were collected, homogenized in PBS, centrifuged at 2,500 × *g* for 20 min at 4°C, and supernatants were collected for subsequent biochemical assays. ATP content (#S0027), mitochondrial transmembrane potential (MMP; #C2006), and reactive oxygen species (ROS; #S0033S) levels were determined using commercial kits from Beyotime Biotechnology. LDH content was measured using commercial kits (#ml911206V) from Enzyme-Linked Biotechnology Co. Ltd. LDH activity (#A020-2) and pyruvate (#A154-1-1) and lactate (#A081-1-1) levels were measured using commercial kits from Nanjing Jiancheng Bioengineering Institute. The nicotinamide adenine dinucleotide/nicotinamide adenine dinucleotide reduced (NAD^+/NADH) ratio was determined using an NAD/NADH-Glo Assay kit (Promega; #G9071). All the investigated indicators were measured according to the instructions of manufacturers and normalized against protein content if necessary. Protein concentrations were determined by the BCA method.

Terminal Deoxynucleotidyl Transferase Deoxynucleotide Triphosphate Nick-End Labeling Assay and Flow Cytometry

Freshly isolated zebrafish testes ($n = 8$–12 testes; 1 testis randomly isolated from each fish) were immediately fixed in 4% PFA overnight at 4°C. After washing three times in PBS for 10 min each time, testes were infiltrated in 30% sucrose at 4°C

overnight and then embedded in tissue freezing medium [i.e., optimal cutting temperature compound (OCT)], followed by cryosectioning using a cryostat (Leica; #CM1860). Terminal deoxynucleotidyl transferase (TdT) deoxynucleotide triphosphate (dUTP) nick-end labeling (TUNEL) assays were conducted using an *in situ* cell death detection kit (Roche; #11684795910), following the manufacturer's protocols. Images were obtained, and TUNEL-positive cell numbers were counted and normalized against to the total area of 4′,6-diamidino-2′-phenylindole (DAPI) stain in each testicular section.

Apoptosis assays of GC-1 cells ($n = 7$–8 wells each group) were performed using an Annexin V-FITC Apoptosis Detection Kit (Dojindo; #AD10), according to the manufacturer's instructions. GC-1 cells in 6-well plates were trypsinized with ethylenediaminetetraacetic acid–free trypsin (Servicebio; #G4013) and collected into centrifuge tubes. The cells were washed three times with PBS and resuspended in 100 μL of binding buffer. Subsequently, 5 μL of Annexin V-FITC and 5 μL of propidium iodide solution were added to each sample. After incubation in darkness for 15 min at room temperature, 20,000 cells of each sample were counted and analyzed using flow cytometry on a Cytoflex S instrument (Beckman Coulter). Data were analyzed by CytExpert software (version 2.4; Beckman).

Immunostaining

Frozen slices of zebrafish testes were obtained as above; then the frozen sections were baked in an oven at 37°C for 10 to 20 min, fixed in 4% PFA for 30 min, and washed with PBS (pH 7.4) three times. Next, the slides were treated for antigen retrieval using citric acid antigen repair solution (Beyotime; #G1202). After washing with PBS, the slides were blocked with 3% bovine serum albumin (BSA; Beyotime; #GC305010) for 30 min at room temperature. The primary antibody rabbit anti-γ H2AX (1:500; GeneTex; #GTX127342) was added to the testes and incubated overnight at 4°C, followed by washing with PBS (pH 7.4) before incubation with a secondary antibody [1:300; Cy3-conjugated goat antirabbit immunoglobulin (IgG); Servicebio; #GB21303] for 50 min in darkness at room temperature. To label the nuclei, the testicular sections were stained with 1 μg/mL of DAPI (Servicebio; #G1012) at 4°C for 10 min after rinsing with PBS. Immunostained testicular tissues were washed, dried, and mounted in 75% antifade mounting medium (1 × PBS, 75% glycerol, 2% *n*-propyl gallate). The slices were viewed under a TCS SP8 time-lapse confocal microscope (Leica) and photographed using a Leica LAS X software imaging system (version 3.7.4; Leica). The positive signal was quantified as the ratio of the fluorescence intensity of target positive signals to the corresponding fluorescence intensity of DAPI in each field. The area was measured using ImageJ software.[58] A series of testicular sections from six individual zebrafish ($n = 6$) were examined for image analysis. In zebrafish, the γ-H2AX signal can be found in spermatocytes at both the leptotene and the zygotene stages owing to meiotic recombination, with the signals being stronger at the leptotene stage than at the zygotene stage.[59] To avoid the interference of meiotic recombination, we distinguished two different stages of spermatocytes (SPC-I: zygotene spermatocytes, signals dispersed within the nucleus; SPC-II: leptotene spermatocytes, strong signals concentrated within in the nucleus) by their shape and density of immunostaining signals,[59] then quantified and compared their expression of γ-H2AX, separately.

Western Blotting Analysis

Total protein lysates were isolated from pooled zebrafish testicular tissues from three fish of the same replicate ($n = 3$; testes of three fish from the same tank were pooled as one replicate sample) or cultured GC-1 cells ($n = 3$; $\sim 5 \times 10^6$ cells each group) with ice-cold radioimmunoprecipitation assay buffer (Beyotime; #P0013B), followed by centrifugation at 12,000 × *g* for 15 min at 4°C. Supernatants were collected, and protein concentrations were determined using the BCA method. The isolated proteins were separated by 10% SDS–polyacrylamide gel electrophoresis (SDS-PAGE), electroblotted onto a polyvinylidene fluoride (PVDF) membrane (Immobilon-P), blocked in 5% nonfat milk on a shaker at room temperature for 2 h, and incubated at 4°C overnight with primary antibodies, including anti-phospho-c-jun N-terminal kinase (anti-p-JNK; 46/54 KDa; 1:1,000; Cell Signaling Technology; #4668T), anti-cleaved-poly (adenosine diphosphosphate [ADP]-ribose) polymerase (anti-cleaved-PARP; 89 KDa; 1:1,000; Cell Signaling Technology; #5625T), anti-cleaved caspase-3 (17 KDa; 1:1,000; Cell Signaling Technology; #9661T), anti-Caspase-3 (32/17 KDa; 1:1,000; Abcam; #Ab13585), anti-caspase-8 (53/40 KDa; 1:1,000; Proteintech; #13423-1-AP), anti-receptor-interacting serine-threonine kinase 3 (anti-RIPK3; 56 KDa; 1:1,000; Affinity; #DF7339), anti-RIPK1 (76 KDa; 1:1,000; Affinity; #AF7877), anti-mixed lineage kinase domain-like protein (anti-MLKL; 54 KDa; 1:1,000; Proteintech; #66675-1-Ig), anti-p-MLKL (54 KDa; 1:1,000; Affinity; #AF7420), and anti-P53 (53 KDa; 1:1,000; Cell Signaling Technology; #2524). After being washed five times with Tris buffered saline with Tween 20 (TBST) solution for 5 min each time, membranes were incubated with secondary antibodies (horseradish peroxidase–conjugated affinipure goat antimouse/antirabbit IgG; 1:10,000; Boster; #BA1051/BA1054) on a shaker at room temperature for 2 h. Enhanced chemiluminescence (ECL) reagent (Pierce) was applied to visualize protein expression, and ImageJ software[58] was used to analyze the expression of target proteins.

Statistical Analysis

Statistical analysis was performed with SPSS software (version 22.0; IBM), and graphs were generated by GraphPad Prism (version 8.0; Graphpad). Data normality and homogeneity of variance were first evaluated by Shapiro–Wilk and Levene's tests, respectively. Then the differences in mean values among control and treatment groups were analyzed by one-way analysis of variance (ANOVA), followed by the post hoc least significant difference (LSD) test. The standard for significance was set as $p < 0.05$. Data are presented as means ± standard errors of the mean (SEMs). A Pearson correlation analysis was conducted between the 1 μM DBDPE-exposure group and the oxamate-exposure group for the investigated parameters in GC-1 cells.

Results

Spermatozoa Motility and Offspring Development in Ex Vivo

First, we performed a pre-experiment to determine exposure concentrations and durations in the formal experiment. The results showed that the 3-h–exposed spermatozoa demonstrated significantly lower TM and PM at 0.01, 0.1, and 1 μM (Figure S1). However, when exposure duration was prolonged to 6 h, significantly lower PM and LIN of zebrafish spermatozoa were observed only in the 0.01 μM DBDPE-exposed zebrafish spermatozoa when compared with control spermatozoa (Figure S1). The pre-experiment results suggested that the spermatozoa seemed to be more sensitive to 3 h of exposure than to 6 h of exposure. Based on the pre-experiment results, *ex vivo* zebrafish spermatozoa exposure to 0.01–10 μM DBDPE for 3 h, followed by artificial fertilization, were performed to evaluate the potential toxicity of DBDPE on spermatozoa and the development of

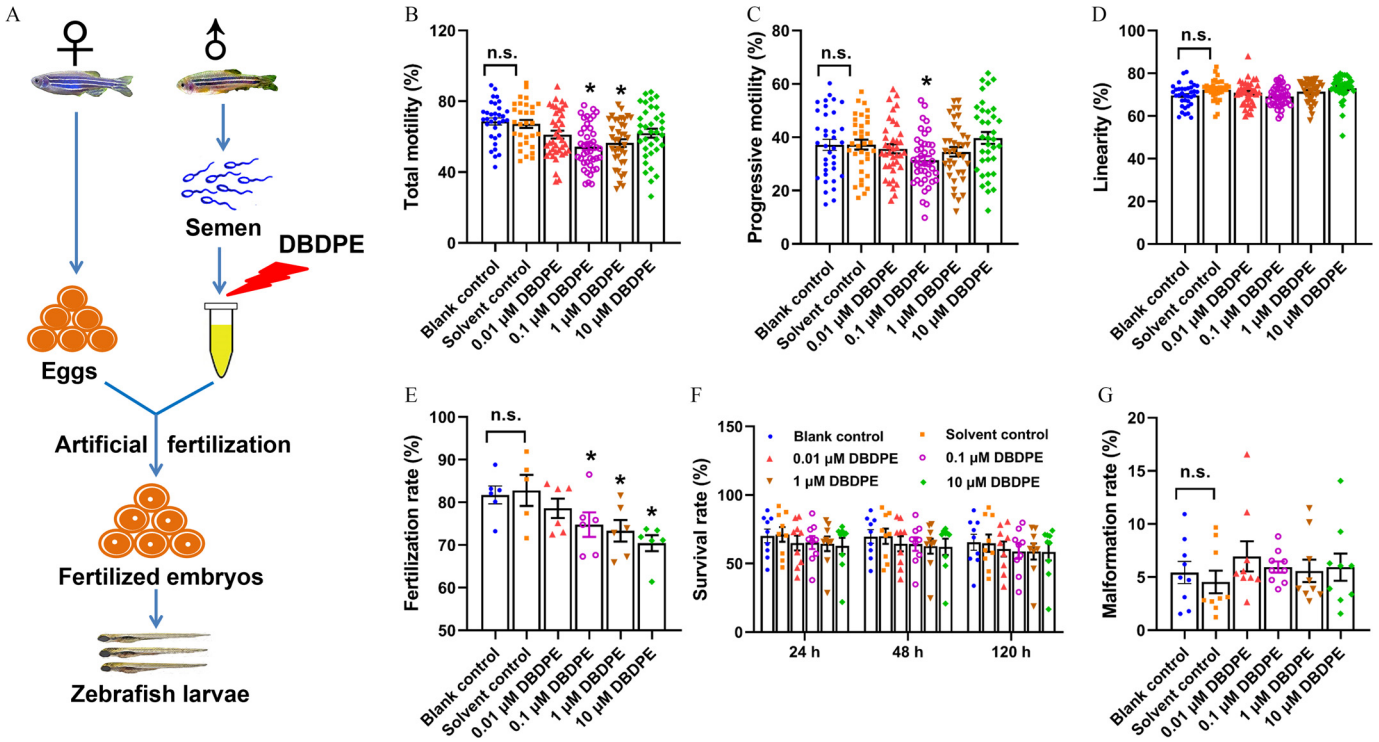

Figure 1. Effects of DBDPE *ex vivo* exposure on zebrafish spermatozoa motility and development of offspring obtained by artificial fertilization. (A) Schematic diagram for *ex vivo* exposure of zebrafish spermatozoa and artificial fertilization. (B) Total motility (TM) of zebrafish spermatozoa. (C) Progressive motility (PM) of zebrafish spermatozoa. (D) Linearity of zebrafish spermatozoa. Each dot in (A–D) represents one replicate data point (mean value of each test sample). The dot numbers represent the data size ($n = 30$–41/group) for statistical analysis. (E) Fertilization rate of zebrafish embryos derived by artificial fertilization using unexposed eggs and DBDPE-exposed sperm ($n = 6$/group). (F) Survival rate determined at 24 h, 48 h, and 120 h post-hatching (hpf) of zebrafish embryos obtained by artificial fertilization ($n = 9$/group). (G) Malformation rate determined at 120 h post-hatching of zebrafish embryos obtained by artificial fertilization ($n = 9$/group). Results are represented as means ± standard errors of the mean (SEMs). See Table S1 for definitions of total and progressive motility and linearity of spermatozoa. Data are reported in Excel Table S1. Note: DBDPE, decabromodiphenyl ethane; DMSO, dimethyl sulfoxide. $^{*}p < 0.05$ indicates a significant difference between DBDPE exposure and solvent control groups, by one-way analysis of variance (ANOVA) followed by the post hoc least significant difference (LSD) test; n.s. indicates no significant difference between blank control and solvent control (0.05% DMSO) groups.

offspring in the formal experiment (Figure 1A). After 3 h of exposure, TM (0.1 and 1 μM) and PM (0.1 μM) of zebrafish spermatozoa were significantly lower than those of the control, but spermatozoa LIN was not significantly different (Figure 1B–D). No significant differences were observed in spermatozoa velocity parameters, including VAP, VCL, and VSL (Figure S2A–C). In addition, when 3-h–exposed zebrafish spermatozoa were artificially fertilized with unexposed zebrafish eggs, significantly lower fertilization rates were observed in the 0.1, 1, and 10 μM DBDPE-exposure groups when compared with the control group (Figure 1E), and survival rates at most time points displayed a concentration-dependent trend toward lower survival, but this was not statistically significant (Figure 1F). Malformation rates (Figure 1G) and hatching rates (Figure S2D) were also not different from control.

DBDPE Contents in Zebrafish Testes

The contents of DBDPE in testes from 2-month–exposed zebrafish were 870.84 ± 98.45, 1,284.2 ± 482.54, 1,410.83 ± 29.09, and 3,252.30 ± 219.40 ng/g lw in the 0.1, 1, 10 and 100 nM DBDPE-exposed groups, respectively. The concentrations of DBDPE in the control testes were below the LOD (Table S4).

Reproductive Behavior and Offspring Development in Zebrafish

After DBDPE exposure, significantly greater body length and condition factor were observed in male zebrafish from the 100 nM-exposure group, and significantly higher body weight was observed in those from the 1 nM-exposure group, whereas no significant differences were observed in GSI in all DBDPE-exposure groups, when compared with the control group (Table S5). When DBDPE-exposed male zebrafish were paired with unexposed female zebrafish, all commonly used reproductive end points, including reproductive behavior (Figure S3) and egg production (Table S5), were unaffected. In F1 offspring larvae, a significantly lower hatching rate was observed only in the 100 nM-exposure group compared with the control group, whereas other parameters, such as fertilization, malformation, and survival rates, were not different from control (Table S5).

Spermatozoa Motility, Ultrastructure, and Gonadal Histology in Zebrafish

After exposure to DBDPE for 2 months, significantly lower TM and PM of zebrafish spermatozoa were observed at all the tested concentrations when compared with the control (Figure 2A,B). Meanwhile, when compared with the control, significantly lower VAP and VCL of zebrafish spermatozoa were observed in fish exposed to 0.1 nM DBDPE, significantly lower VSL was observed in fish exposed to both 0.1 and 100 nM DBDPE, and the fish exposed to 100 nM DBDPE demonstrated significantly lower spermatozoa LIN (Figure 2C–F). Furthermore, the scanning electron microscopy results showed no obvious effects on spermatozoa tail length following DBDPE exposure (Figure 2I), but the males exposed to 1 and 100 nM DBDPE demonstrated significantly shorter spermatozoa head length than those in the control group (Figure 2J), and significantly

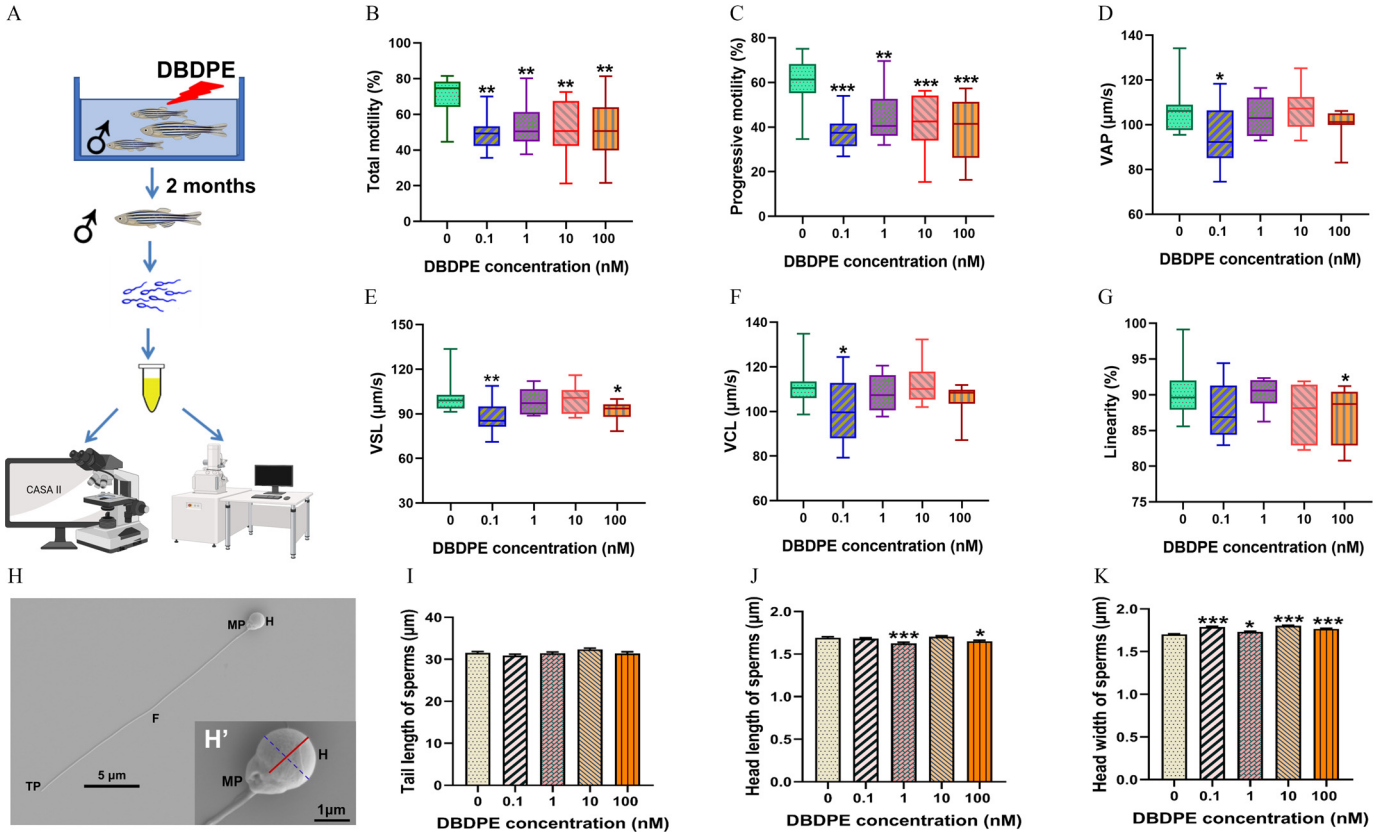

Figure 2. Effects of DBDPE *in vivo* exposure on motility parameters and ultrastructure morphology of zebrafish spermatozoa. (A) Schematic diagram of collecting sperm after *in vivo* exposure of zebrafish for spermatozoa motility and ultrastructural imaging. The illustration was in part created in BioRender (2024) https://BioRender.com/o11a377. (B) Total motility (TM; %) of spermatozoa ($n = 9$–10). (C) Progressive motility (PM; %) of spermatozoa ($n = 9$–10). (D) Average path velocity (VAP; μm/s) of spermatozoa ($n = 9$–10). (E) Straight-line velocity (VSL; μm/s) of spermatozoa ($n = 9$–10). (F) Curvilinear velocity (VCL; μm/s) of spermatozoa ($n = 9$–10). (G) Linearity (LIN; %) of spermatozoa ($n = 9$–10). Box plots represent the median values with upper and lower quartiles; whiskers extend to the maximum to minimum. (H) Typical spermatozoa (normal spermatozoa from control group) morphology observed by scanning electron microscope. (H′) Magnification of a typical zebrafish spermatozoa head. The solid red line indicates head length, and the dotted blue line indicates head width measured in the present study. (I) Spermatozoa tail length measured in each group. (J) Spermatozoa head length measured in each group. (K) Spermatozoa head width measured in each group. Ten semen samples were assessed for different spermatozoa motility parameters in each group. Zebrafish spermatozoa ($n = 78$–96 spermatozoa/group) were randomly selected for measurement of tail length, head length, and head width in each group. Results are represented as means ± standard errors of the mean (SEMs). See Table S1 for definitions of TM, PM, VAP, VSL, VCL, and LIN. Data are reported in Excel Table S2. Note: CASA, computer-assisted sperm analysis; DBDPE, decabromodiphenyl ethane; F, flagellum; H, head; MP, midpiece; TP, terminal piece. $^{*}p < 0.05$, $^{**}p < 0.01$, and $^{***}p < 0.001$ indicate significant differences between exposure and control groups, by one-way analysis of variance (ANOVA) followed by the post hoc least significant difference (LSD) test.

greater spermatozoa head width was observed in fish exposed to DBDPE at all investigated concentrations (Figure 2K).

H&E staining showed that germ cells at different developmental stages were present in the testes of each group, including spermatogonia (SG), spermatocytes (SPC), and spermatozoa (SPD; Figure 3A–E). A slight wider interstitial space was observed especially upon DBDPE exposure at higher concentrations (1, 10, and 100 nM), although no significant difference was observed compared with control (Figure 3F and Figure S4; $p = 0.149$, 0.056, and 0.116, respectively). Semiquantitative measurement showed that the 100 nM DBDPE-exposure group demonstrated a significantly lower percentage of relative areas occupied by SPD compared with the control group, whereas both the 1 and 100 nM DBDPE-exposure groups showed significantly higher percentages of relative areas occupied by spermatogonia (SPG) (Figure 3F).

Whole-Proteome and Phosphoproteome Analyses in Zebrafish Testes

Quantitative proteomics integrating whole-proteome and phosphoproteome approaches were applied to explore differences in expression and phosphorylation profiles of global proteins between control and 100 nM DBDPE-exposed zebrafish testes (Figure 4A). In total, we obtained 10,274 proteins from whole-proteome analysis and 7,250 phosphorylation sites on 4,418 proteins from phosphoproteome (<1% FDR) analysis. Phosphorylation sites are shown in Figure S5A. Specifically, 457 DEPs (226 up-regulated and 231 down-regulated) and 2,110 phosphosites (1,527 on 487 proteins up-regulated and 583 on 239 proteins down-regulated) were identified in 100 nM DBDPE-treated testes compared with controls (Figure 4B; Figure S5B,C).

KEGG analysis of DEPs revealed that DBDPE exposure was associated with proteins in the necroptosis, phosphatidylinositol signaling system, ubiquinone, and other terpenoid–quinone biosynthesis categories (Figure 4D). KEGG enrichment analysis of phosphoproteins harboring differentially phosphorylated sites revealed that pathways, including base excision repair, homologous recombination, mismatch repair, and DNA replication, were associated with DBDPE exposure (Figure 4E). GO analysis of both whole-proteome and phosphoproteome data revealed that organelle organization and cellular component organization were enriched (Figure 5E; Figure S5D). Other biological processes,

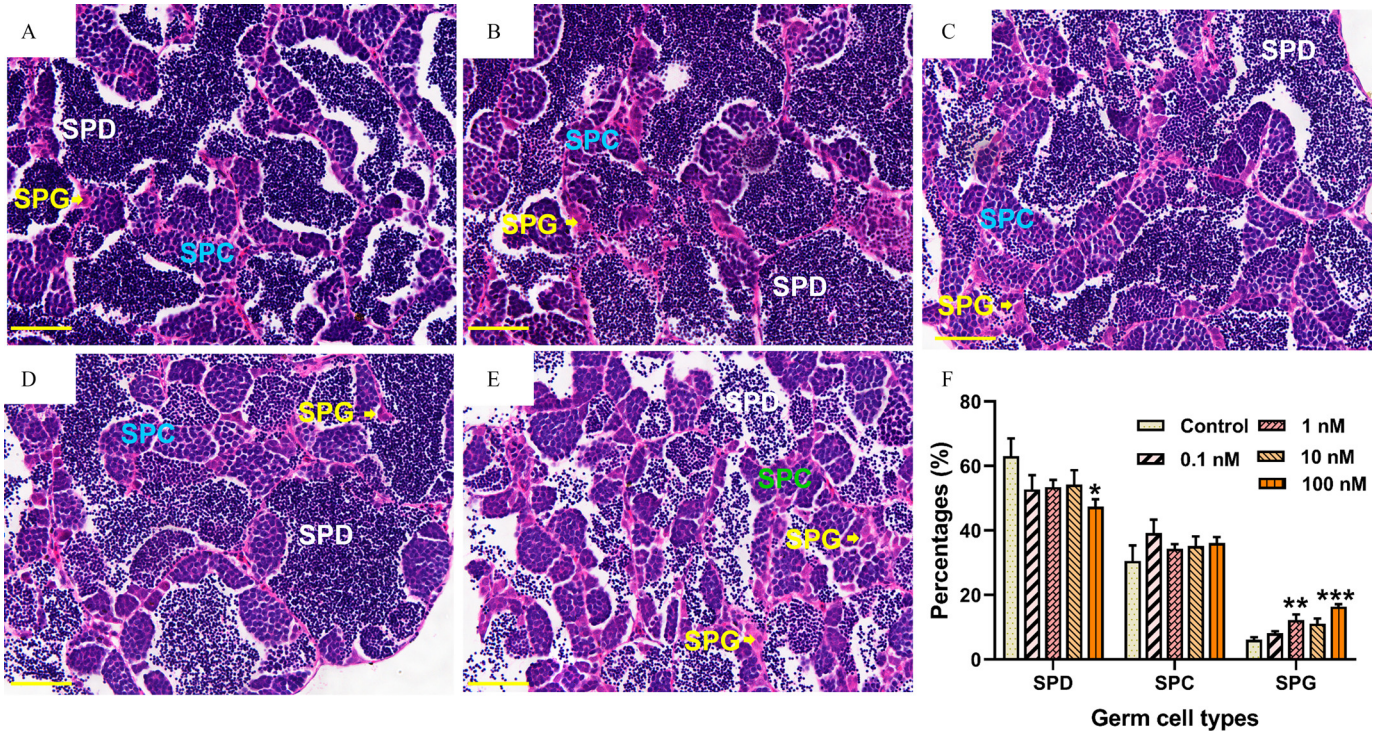

Figure 3. Histological observations of male zebrafish testes after 2-month *in vivo* exposure to DBDPE. (A–E) Typical hematoxylin/eosin–stained sections of testes in 0, 0.1, 1, 10, and 100 nM-exposure groups, respectively. (F) Proportion quantification of germ cells at different developmental stages in testes ($n = 6$–9 fish/group). Results are represented as means ± standard errors of the mean (SEMs). Scale bar: 50 μm. Data are reported in Excel Table S3. Note: DBDPE, decabromodiphenyl ethane; SPC, spermatocytes; SPD, spermatozoa; SPG, spermatogonia. $^{*}p < 0.05$, $^{**}p < 0.01$, and $^{***}p < 0.001$ indicate significant differences between exposure and control groups, by one-way analysis of variance (ANOVA) followed by the post hoc least significant difference (LSD) test.

such as histone deacetylation and protein deacetylation, were enriched in proteome data according to GO analysis (Figure S5D), and chromosome organization, chromatin organization, and DNA repair were also enriched in phosphoproteome data (Figure S5E).

As indicated in the PPI network (Figure 4F; Excel Table S4), expression levels of inositol 1,4,5-trisphosphate receptors ITPR1A [$\log_2$(fold change) = −5.04] and ITPR3 [$\log_2$(fold change) = −5.04] along the inositol triphosphate/calcium ion (IP3/Ca^{2+}) signaling pathway were significantly lower than in control, and proteins related to phosphatidylinositol (3,4,5)-trisphosphate (PIP3) decomposition [inositol monophosphatase 2 (IMPA2); $\log_2$(fold change) = 2.29] and PIP2 synthesis [phosphatidylinositol-4-phosphate 5-kinase, type I, alpha, b (PIP5K1AB); $\log_2$(fold change) = 1.87; 1-phosphatidylinositol-3-phosphate 5-kinase (PIKFYVE); $\log_2$(fold change) = 1.26] were significantly higher, but the phosphorylation level of AKT1 substate 1 [AKT1S1; $\log_2$(fold change) = −1.54] was significantly lower. In addition, less glycolysis was observed in DBDPE-exposed fish testes, as indicated by lower expression levels of the dihydrolipoamide acetyltransferase component of pyruvate dehydrogenase complex [PDHX; $\log_2$(fold change) = −1.27] and pyruvate kinase L/R [PKLR; $\log_2$(fold change) = −0.98] and lower phosphorylation levels of lactate dehydrogenase Ba [LDHBA; $\log_2$(fold change) = −1.06] and aldolase a [ALDOAA; $\log_2$(fold change) = −1.46]. Greater oxidative phosphorylation was observed in DBDPE-exposed fish testes, as shown by higher expression levels of proteins such as NADH dehydrogenase (ubiquinone) 1 subunit C2 [NDUFC2; $\log_2$(fold change) = 0.77] and ubiquinol-cytochrome C reductase core protein 2b [UQCRC2B; $\log_2$(fold change) = 0.62] and higher phosphorylation levels of proteins, such as ATP synthase peripheral stalk subunit d [ATP5PD; $\log_2$(fold change) = 7.63] and solute carrier family 25 member 5 [SLC25A5; $\log_2$(fold change) = 2.51].

Transcriptional Profiles in Zebrafish Testes

The transcriptional profiles of representative genes in the proposed pathways from the proteome and phosphoproteome analysis were determined in zebrafish testes by qRT-PCR to see whether those pathways were also affected at lower concentrations (0.1, 1, and 10 nM). As shown in Figure S6 and Excel Table S15, exposure to DBDPE at concentrations of 1 and 10 nM resulted in significantly lower transcription levels of the cell death-associated gene *caspase9*, whereas the transcription of *ripk3*, another crucial gene in cell death pathways, demonstrated higher levels at 0.1 and 1 nM. Among genes associated with the DNA damage response, the transcription of *parp1*, *parp2*, *parp3*, *pold1*, *pold3*, *lig3*, and *tp53bp1* demonstrated an upward trend after exposure to lower concentrations of DBDPE; the transcription of *brca2*, *brat1*, and *mcm2* demonstrated an upward trend at 0.1 nM, but a downward trend at 10 nM. The transcription levels of genes (*cdk10*, *cdk11b*, *cdk12*, *cdk13*) regulating the cell cycle and genes (*jak3*, *akt1s1*, *pik3c2a*, and *pik3r1*) related to the Janus kinase/phosphoinositide 3-kinase/protein kinase B (JAK/PI3K/AKT) pathways were higher after exposure to 0.1–10 nM DBDPE. The transcription levels of genes related to oxidative phosphorylation (*ndufc2*, *uqcrc2b*, *atp6voe1*, *atp5l*, *slc25a5*, *coq5*, and *coq6*) were higher after exposure to 0.1–10 nM DBDPE, whereas the transcription levels of the glycolysis-related genes *pkma* and *adh8a* demonstrated a downward trend in these exposure groups.

DNA Damage and Apoptosis in Zebrafish Testes

We used a typical marker (the histone protein γ-H2AX) for DNA double-strand breaks (DSBs) to test whether DBDPE exposure was associated with DNA damage in the testicular germ cells via

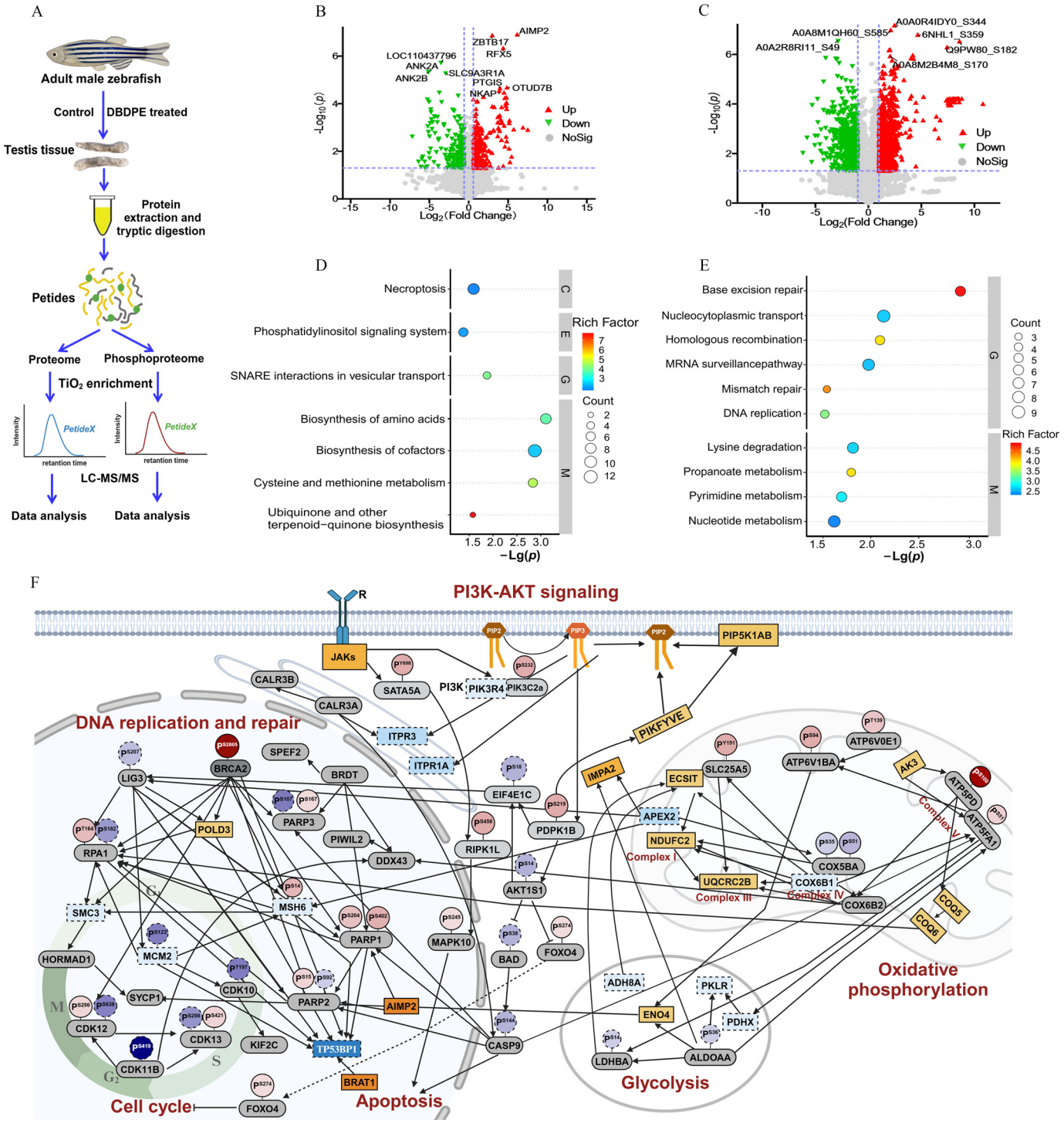

Figure 4. Whole-proteome and phosphoproteome analysis of male zebrafish testes after *in vivo* exposure to 100 nM DBDPE. (A) Schematic diagram of proteome and phosphoproteome analysis. The illustration was in part created in BioRender (2024) https://BioRender.com/x32w463. (B) Volcano plot of quantified proteins in 100 nM DBDPE-treated zebrafish testes. (C) Volcano plot of quantified phosphosites in 100 nM DBDPE-treated zebrafish testes. Upward triangle (filled in red; on the upper right corner) and upside-down triangle (filled in green; on the upper left corner) in (B) and (C) indicate up-regulation and down-regulation, respectively; gray dots indicate no significant difference. (D) Significantly enriched KEGG pathways of differentially expressed proteins (DEPs) from whole-proteome data. (E) Significantly enriched KEGG pathways of proteins harboring differentially phosphorylated sites from phosphoproteome data. The size of the dots in (D) and (E) represents the number of DEPs in the pathway, and the color of the dots represents the enrichment factors of KEGG pathway. (F) Protein–protein interaction (PPI) network after exposure to 100 nM DBDPE. The illustration was created in BioRender (2023) https://BioRender.com/o93k219. Each large oval represents protein expression level, and smaller ovals with a tail on top represent phosphorylation levels of specific phosphorylation sites of the protein. Solid line boxes and dotted line boxes respectively indicate up-regulation and down-regulation in the proteome; gray-filled ovals indicate proteins without significant differences. Solid line circles and dotted line circles respectively indicate up-regulation and down-regulation in the phosphoproteome. Color intensity is proportional to $\log_2$ (fold change). Data are reported in Excel Table S4. Note: DBDPE, decabromodiphenyl ethane; KEGG, Kyoto Encyclopedia of Genes and Genomes; PI3K-AKT, phosphoinositide 3-kinase/protein kinase B; SNARE, soluble *N*-ethylmaleimide-sensitive factor attachment protein receptor; TiO_2, titanium dioxide.

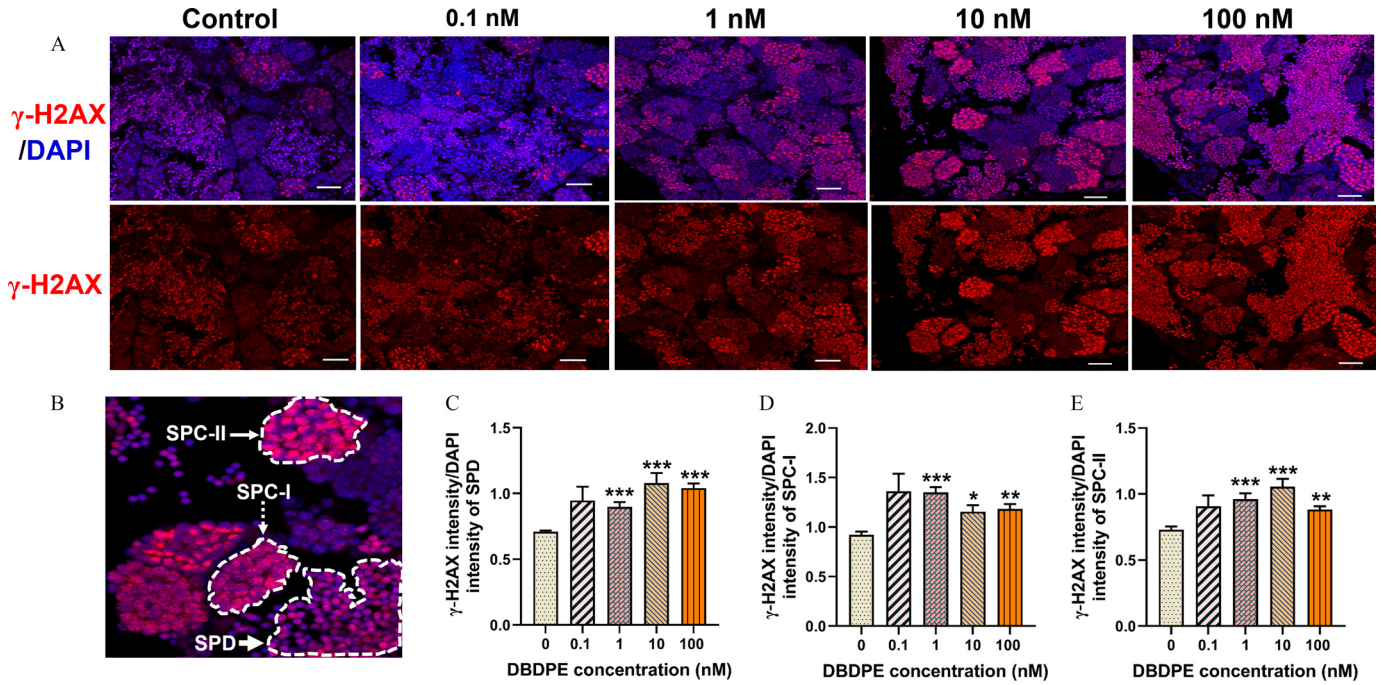

Figure 5. DNA damage in zebrafish testes exposed to DBDPE *in vivo*. (A) DNA damage in zebrafish testes detection by immunofluorescence staining against the histone protein γ-H2AX. The representative images show DAPI-stained (blue) nuclei with nuclear γ-H2AX foci in red. Scale bar: 20 μm. (B) Representative positive signals detected in SPD (indicated by white bold arrow), SPC-I (indicated by white dashed arrow; zygotene spermatocytes, signals dispersed within the nucleus), and SPC-II (indicated by white thin arrow; leptotene spermatocytes, strong signals concentrated within in the nucleus). (C) Ratio of fluorescence intensity of γ-H2AX to the corresponding fluorescence intensity of DAPI in SPD. (D) Ratio of fluorescence intensity of γ-H2AX signals to the corresponding fluorescence intensity of DAPI in SPC-I. (E) Ratio of fluorescence intensity of γ-H2AX signals to the corresponding fluorescence intensity of DAPI in SPC-II. Results are represented as means ± standard errors of the mean (SEMs), $n = 6$ testes. Data are reported in Excel Table S5. Note: DAPI, 4′,6-diamidino-2′-phenylindole; DBDPE, decabromodiphenyl ethane; SPC, spermatocytes; SPD, spermatozoa. $^{*}p < 0.05$, $^{**}p < 0.01$, and $^{***}p < 0.001$ indicate significant differences between exposure and control groups, by one-way analysis of variance (ANOVA) followed by the post hoc least significant difference (LSD) test.

immunofluorescence staining. Significantly higher relative florescence density of γ-H2AX was observed in SPD, SPC-I, and SPC-II in the testes of fish exposed to 1, 10, and 100 nM DBDPE (Figure 5A–E). We subsequently found a significantly higher number of TUNEL-positive cells in the testes of zebrafish exposed to 100 nM DBDPE compared with those in the control (Figure 6A,B). We also evaluated key proteins mediating the responses to DNA damage (cleaved PARP) and those contributing to cell apoptosis (cleaved caspase-3, P-JNK) by Western blotting (Figure 6C), and DBDPE-exposed zebrafish testes presented significantly higher expression levels of cleaved PARP, cleaved caspase-3, and both P-JNK-1 and P-JNK-2 compared with control fish (Figure 6D).

Energy Metabolic Level in Zebrafish Testes

Integrated whole-proteome and phosphoproteome analysis also indicated energy metabolism differences in zebrafish testes following DBDPE exposure. The fish exposed to DBDPE at all investigated concentrations demonstrated a significantly lower NAD^+/NADH ratio in testicular tissues compared with that in the control (Figure 7A). Significantly higher MMP in testes was observed in fish following exposure to 0.1, 10, and 100 nM DBDPE compared with the control (Figure 7B). Exposure to DBDPE at 1 and 100 nM also resulted in a significantly higher ATP content in testes (Figure 7C). However, no obvious differences were observed in ROS levels in testes following DBDPE exposure (Figure 7D). The glucose content in testes exhibited a dose-dependent accumulation upon DBDPE exposure, with significantly higher content observed at the highest concentration compared with that in the control (Figure 7E). A significantly lower lactate/pyruvate ratio was observed in testes following DBDPE exposure at all concentrations (Figure 7F). Furthermore, when compared with the control, lower levels of LDH content and LDH activity in testicular tissues were found in DBDPE-exposed fish, with significances observed at 10 and 100 nM for LDH content, as well as at 1 and 100 nM for LDH activity (Figure 7G,H).

DNA Damage and Energy Metabolism in GC-1 Cells

We further validated the DNA damage, apoptosis, and metabolic changes observed in zebrafish testicular tissues using mouse spermatogonial GC-1 cells. First, a pre-experiment was performed to determine exposure concentrations and duration by investigating effects of a series of concentrations of DBDPE (0.01–10 μM) on MMP and ATP contents in GC-1 cells. After a 48-h exposure of DBDPE, MMP was significantly higher at 0.1 and 1 μM, whereas ATP was significantly higher only at 1 μM, with no significant differences observed at both 0.01 and 10 μM (Figure S7). Therefore, two DBDPE concentrations (0.1 and 1 μM) were selected for further research, and the exposure duration was prolonged to 72 h. The results from the formal experiment showed that exposure to 1 μM DBDPE and oxamate for 72 h resulted in significantly higher γ-H2AX foci formation compared with the control (Figure 8A,B). Consistent with these results, the expression levels of proteins in response to DNA damage, such as cleaved PARP and P53, were up-regulated by DBDPE and oxamate, and statistically significant differences were observed in GC-1 cells following exposure to both concentrations of DBDPE and oxamate for cleaved PARP (Figure 8D–G). Next, we evaluated cell apoptosis by flow cytometry (FCM), and no significant alterations were found in GC-1 cells following DBDPE or

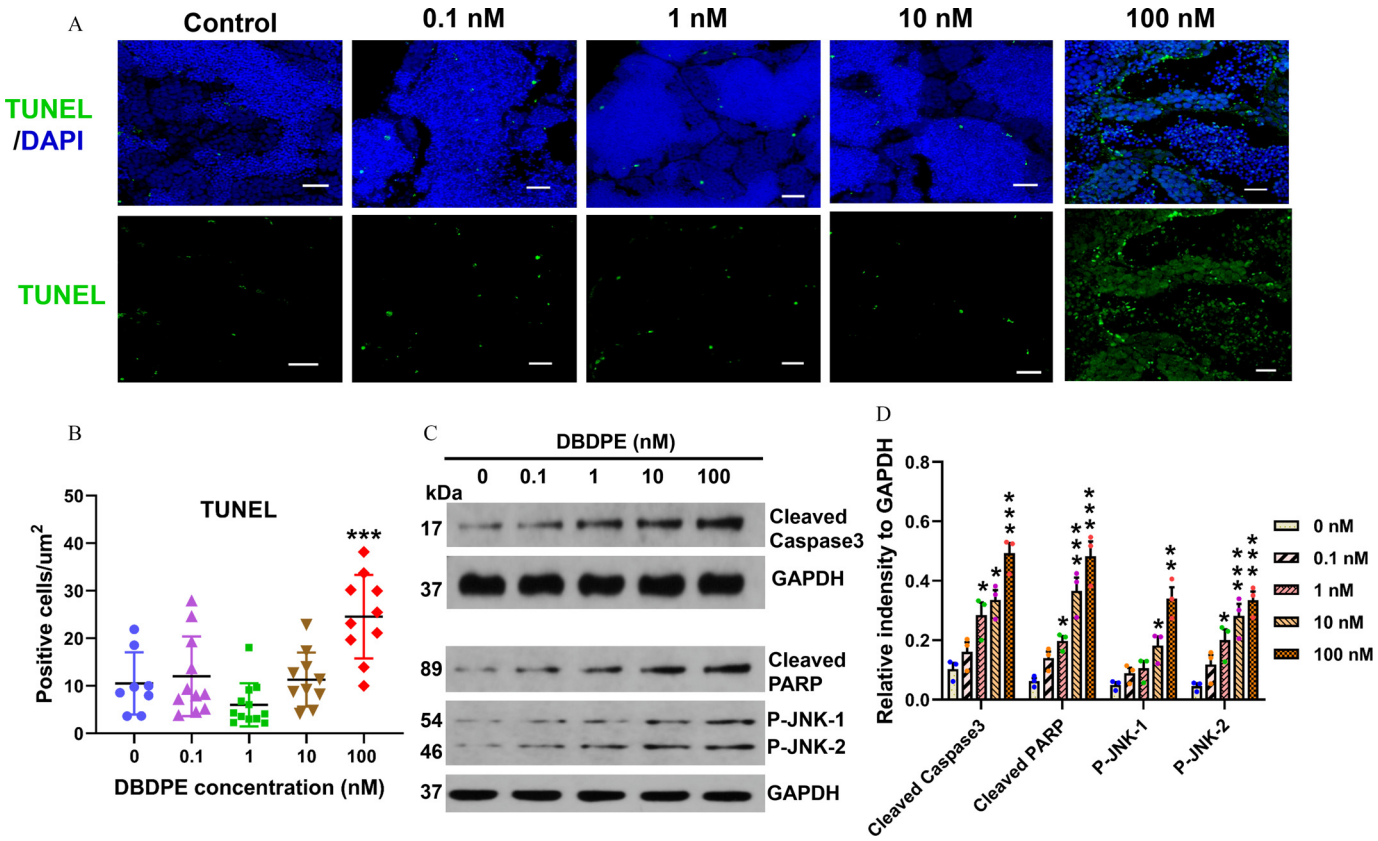

Figure 6. Germ cell apoptosis and expression of proteins related to cell apoptosis in zebrafish testes exposed to DBDPE *in vivo*. (A) Apoptosis detection in zebrafish testes by immunofluorescence staining using TUNEL assay. The representative images show DAPI-stained (blue) nuclei with TUNEL-positive signals in green. Scale bar: 20 μm. (B) Statistical analysis of the total number of TUNEL-positive cells relative to the section areas. Each dot in (B) represents one replicate data point (mean value of each testis). The dot numbers represent the data size ($n = 8$–12) for statistical analysis. (C) Western blotting analyses using antibodies against cleaved caspase-3, cleaved PARP, p-JNK, and GAPDH in testes tissues. The numbers on the left represent molecular weight. (D) Quantification of the abundances of proteins relative to GAPDH ($n = 3$). Results are represented as means ± standard errors of the mean (SEMs). Data are reported in Excel Table S6. Note: DAPI, 4′,6-diamidino-2′-phenylindole; DBDPE, decabromodiphenyl ethane; GAPDH, glyceraldehyde-3-phosphate dehydrogenase; PARP, poly(adenosine diphosphophosphate-ribose) polymerase; p-JNK, phospho-c-jun N-terminal kinase; TUNEL, terminal deoxynucleotidyl transferase deoxynucleotide triphosphate nick-end labeling (assay). $^{*}p < 0.05$, $^{**}p < 0.01$, and $^{***}p < 0.001$ indicate significant differences between exposure and control groups, by one-way analysis of variance (ANOVA) followed by the post hoc least significant difference (LSD) test.

oxamate exposure (Figure 8C). However, Western blot analysis showed that expression levels of protein markers for cell apoptosis, such as cleaved caspase-8 and both P-JNK-1 and P-JNK-2, were significantly up-regulated in GC-1 cells upon exposure to 1 μM DBDPE and oxamate, whereas expression levels of cleaved caspase-3 were also significantly up-regulated by oxamate exposure, and 1 μM DBDPE up-regulated the expression levels of cleaved caspase-3, but not significantly (Figure 8D–G). Furthermore, several protein markers for necroptosis, including RIPK3, RIPK1, and p-MLKL, were also significantly up-regulated in GC-1 cells following exposure to 1 μM DBDPE and oxamate, with the exception of RIPK1 at 1 μM DBDPE (Figure 8H,I).

We also investigated energy metabolism changes in GC-1 cells following DBDPE and oxamate exposure. Similar to the results observed in zebrafish testes, glucose content was higher in cells exposed to either DBDPE or oxamate, but this difference was not statistically significant (Figure 9A). In GC-1 cells exposed to DBDPE at the two investigated concentrations or oxamate, significantly lower LDH activity and higher MMP were observed compared with those in the control, but ROS levels were not different from control (Figure 9B–D), consistent with the results observed in zebrafish testes following DBDPE exposure. To measure the ATP content and further explore the effects of DBDPE and oxamate on glycolysis and oxidative phosphorylation, Seahorse Real-Time ATP Rate assays were performed (Figure 9E). The results suggested that oxamate exposure resulted in significantly higher basal respiration of GC-1 cells, but neither concentration of DBDPE was associated with differences in basal respiration (Figure 9F). However, consistent with the result of oxamate exposure, GC-1 cells exposed to both concentrations of DBDPE demonstrated a significantly higher mitoATP/glycoATP ratio (Figure 9G). The overall results indicate that the lower LDH activity might be driven by a metabolic shift from glycolysis to oxidative phosphorylation in GC-1 cells (Figure 9H). Furthermore, most of the investigated parameters in GC-1 cells were significantly different in the 1 μM DBDPE- and oxamate-exposure groups, compared with controls, and the changing trends were similar. To investigate the relationship between these similarities, a Pearson correlation analysis was performed, and the correlation coefficients of most of the investigated parameters ranged from 0.804 to 0.999 (Figure S8), suggesting positive correlations for changes in the investigated parameters between DBDPE- and oxamate-exposure groups.

Discussion

DBDPE is among the most widely used and predominant NBFRs in various environments,[9,60] and it poses significant exposure

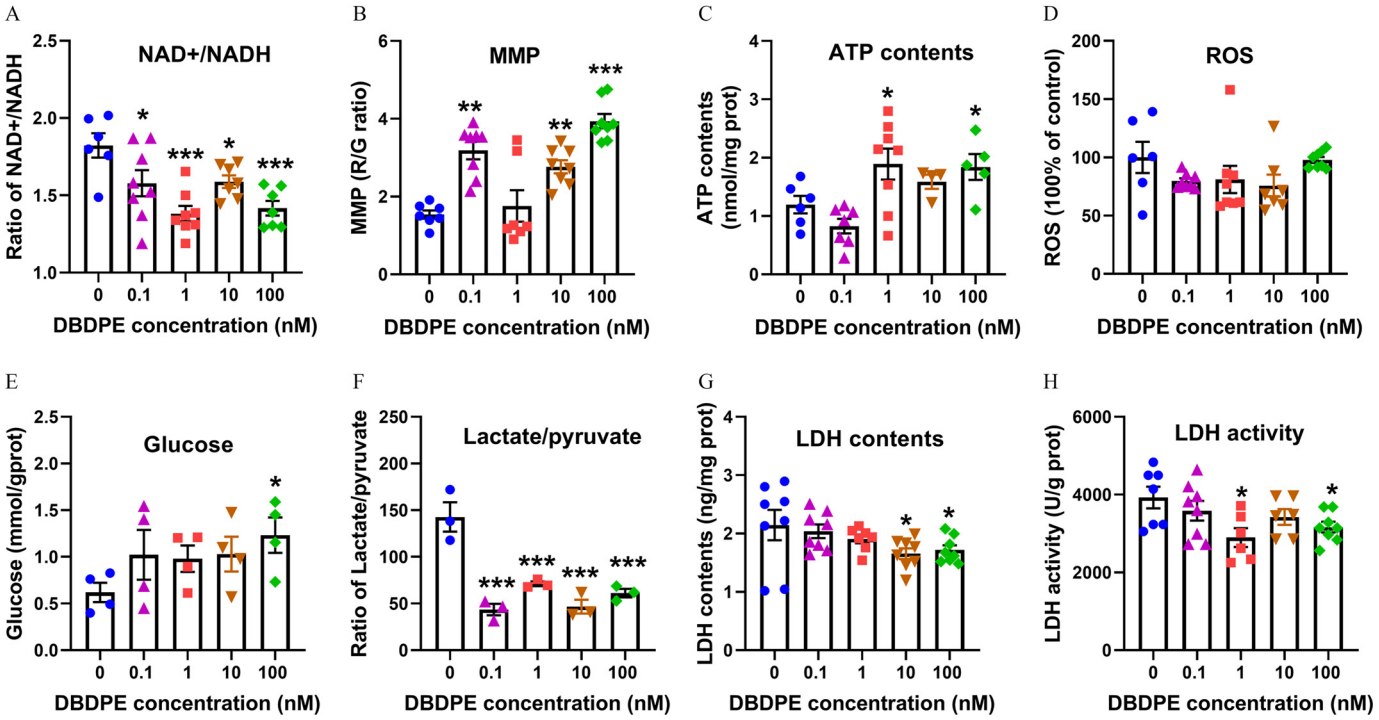

Figure 7. Energy metabolic level in zebrafish testes exposed to DBDPE *in vivo*. (A) NAD^+/NADH ratio in testicular tissues ($n = 6$–8). (B) Mitochondrial membrane potential (MMP) of testicular tissues ($n = 7$–8). (C) ATP content in testicular tissues ($n = 4$–8). (D) ROS levels in testicular tissues ($n = 6$–8). (E) Glucose levels in testicular tissues ($n = 4$). (F) Intracellular lactate/pyruvate ratio in testicular tissues ($n = 3$). (G) LDH content in testicular tissues ($n = 7$–8). (H) LDH activity in testicular tissues ($n = 6$–8). Each dot in (A–H) represents one replicate data point. Results are represented as means ± standard errors of the mean (SEMs). Data are reported in Excel Table S7. Note: ATP, adenosine triphosphate; DBDPE, decabromodiphenyl ethane; G, green; LDH, lactate dehydrogenase; NAD^+, nicotinamide adenine dinucleotide; NADH, nicotinamide adenine dinucleotide reduced; R, red; ROS, reactive oxygen species. $^*p < 0.05$, $^{**}p < 0.01$, and $^{***}p < 0.001$ indicate significant differences between exposure and control groups, by one-way analysis of variance (ANOVA) followed by the post hoc least significant difference (LSD) test.

risks to humans,[21,61] as well as to domestic[62,63] and wild animals.[64] In the present study, we found using an *ex vivo* zebrafish spermatozoa model that DBDPE-exposed spermatozoa demonstrated poorer quality, and this was confirmed in subsequent *in vivo* experiments. Analysis integrating whole-proteome and phosphoproteome approaches in zebrafish testes was employed to profile typical responses from DNA damage to cell death. Interestingly, we observed unexpected mitochondrial hyperpolarization (MHP; significantly higher MMP) and no differences in ROS levels in both zebrafish testicular tissues and GC-1 cells, suggesting the existence of a dosage window before DBDPE may lead to cell death. Moreover, energy reprogramming by shifting glycolysis to oxidative phosphorylation was demonstrated in GC-1 cells. The results suggest male reproductive toxicity of DBDPE and provide new insights into the underlying mechanisms.

Spermatozoa Motility and Offspring Development in Ex Vivo

Spermatozoa motility is an important indicator widely used to characterize male reproductive toxicity, and it is highly sensitive to xenobiotics exposure.[48,65] Therefore, we first performed *ex vivo* zebrafish spermatozoa exposure followed by artificial fertilization to preliminarily evaluate the potential male reproductive toxicity of DBDPE. The TM and PM of zebrafish spermatozoa were significantly lower after 3 h of DBDPE exposure compared with those in control, suggesting impairment of sperm quality. However, the trajectory characteristics of zebrafish spermatozoa were not affected, possibly because they are less sensitive to chemicals owing to fish spermatozoa typically moving via a straight or slightly curved trajectory with a symmetrical flagellar wave.[66] Fertilization success, which is closely related to sperm quality, has long been used as an important indicator of male reproductive toxicity.[67] In the present study, when DBDPE-exposed zebrafish spermatozoa were used for artificial fertilization with healthy zebrafish eggs, fertilization rates were significantly lower, which can be explained by declining spermatozoa motility, as described above. Furthermore, the survival rates of offspring generated from DBDPE-exposed spermatozoa were lower, although this difference was not statistically significant. This may be related to the low concentrations and limited duration of DBDPE exposure, which are key elements determining the toxic effects.

Evaluation of Male Reproductive Toxicity in Vivo

Based on the *ex vivo* results, an *in vivo* DBDPE exposure experiment of male zebrafish was conducted to further investigate its male reproductive toxicity. After a 2-month exposure to DBDPE, we did not observe significant differences in several commonly used indicators, including mating behavior and reproductive success (egg production, fertilization rate, malformation rate, and survival rate of offspring larvae). These results suggest lower male reproductive toxicity of DBDPE compared with traditional BFRs.[68–70] Regardless, the significantly lower hatching rate at 72 hpf indicated potential adverse effects on sperm quality given that hatching rate is the only characteristic inherited from exposed males. As expected, the TM and PM of zebrafish spermatozoa were also significantly lower, and the trajectory characteristics of spermatozoa, including VAP, VCL, and VSL, were also different than control. Furthermore, a smaller head length

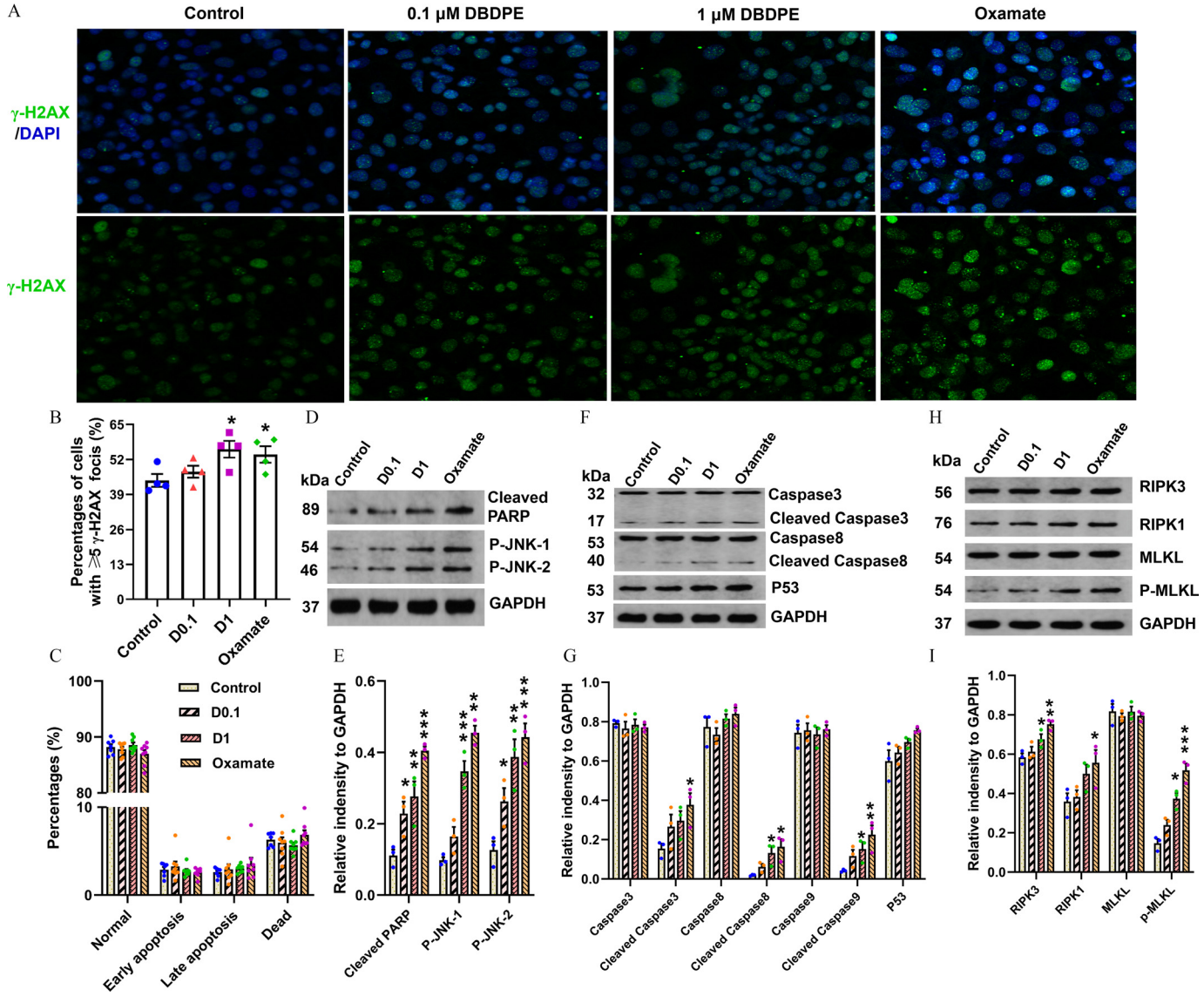

Figure 8. DNA damage and expression of proteins related to apoptosis or necroptosis in mouse spermatogonial GC-1 cells exposed to DBDPE and oxamate (LDH inhibitor) *in vitro*. (A) DNA damage in zebrafish testes detection by immunofluorescence staining against the histone protein γ-H2AX. The representative images show DAPI-stained (blue) nuclei with nuclear γ-H2AX foci in green. (B) Percentages of GC-1 cells with ≥5 γ-H2AX foci ($n = 4$). (C) Cell apoptosis detection by flow cytometry (FCM) using an Annexin V-FITC Apoptosis Detection Kit ($n = 7$–8). (D) Western blotting analyses carried out with antibodies against caspase-3, cleaved caspase-3, caspase-8, cleaved caspase-8, P53, and GAPDH in GC-1 cells. (E) Western blotting analyses carried out with antibodies against cleaved PARP, p-JNK, and GAPDH in GC-1 cells. (F) Western blotting analyses carried out with antibodies against RIPK3, RIPK1, MLKL, p-MLKL, and GAPDH in GC-1 cells. (H–I) Quantification of the abundances of proteins relative to GAPDH ($n = 3$). Each dot in (E–I) represents one replicate data point (one well of cells/replicate). The dot numbers represent the data size for statistical analysis. Results are represented as means ± standard errors of the mean (SEMs). Data are reported in Excel Table S8. Note: DBDPE, decabromodiphenyl ethane; FITC, fluorescein isothiocyanate; glyceraldehyde-3-phosphate dehydrogenase; LDH, lactate dehydrogenase; MLKL, mixed lineage kinase domain-like; PARP, poly(adenosine diphosphosphate-ribose) polymerase; p-JNK, phospho-c-jun N-terminal kinase; RIPK, receptor-interacting serine-threonine kinase 3. $^{*}p < 0.05$, $^{**}p < 0.01$, and $^{***}p < 0.001$ indicate significant differences between exposure and control groups, by one-way analysis of variance (ANOVA) followed by the post hoc least significant difference (LSD) test.

and larger head width of spermatozoa were observed following DBDPE exposure. These results suggested that DBDPE can impair spermatozoa quality in zebrafish. Similarly, DBDPE treatment (50 and 500 mg/kg per day) significantly decreased the density and motility of sperm and increased the occurrence of abnormal sperm in male rats.[36] Disrupted spermatogenesis is usually accompanied by a decline in semen quality following exposure to environmental pollutants.[71,72] In this study, GSI and the interstitial space did not significantly differ between exposed and control fish. In contrast to our study, histopathological damage in testes in the form of seminiferous epithelium deletion was induced by exposure to DBDPE (50 and 500 mg/kg per day) in the rat.[36] In the present study, the proportion of SPG was significantly greater in the 1 and 100 nM DBDPE-exposed fish, and that of SPD was significantly lower in the 100 nM DBDPE-exposed fish, with a lower trend in the fish exposed to 0.1–10 nM DBDPE, which might suggest inhibition of spermatogenesis following DBDPE exposure.

To comprehensively reveal the underlying mechanism of DBDPE-induced male reproductive toxicity, an integrated whole-proteome and phosphoproteome analysis was performed in zebrafish testes, comparing control and 100 nM DEBDPE-exposed groups. KEGG analysis of DEPs revealed that the biological processes of necroptosis ($p = 0.025557$, top 5; Excel Table S4)

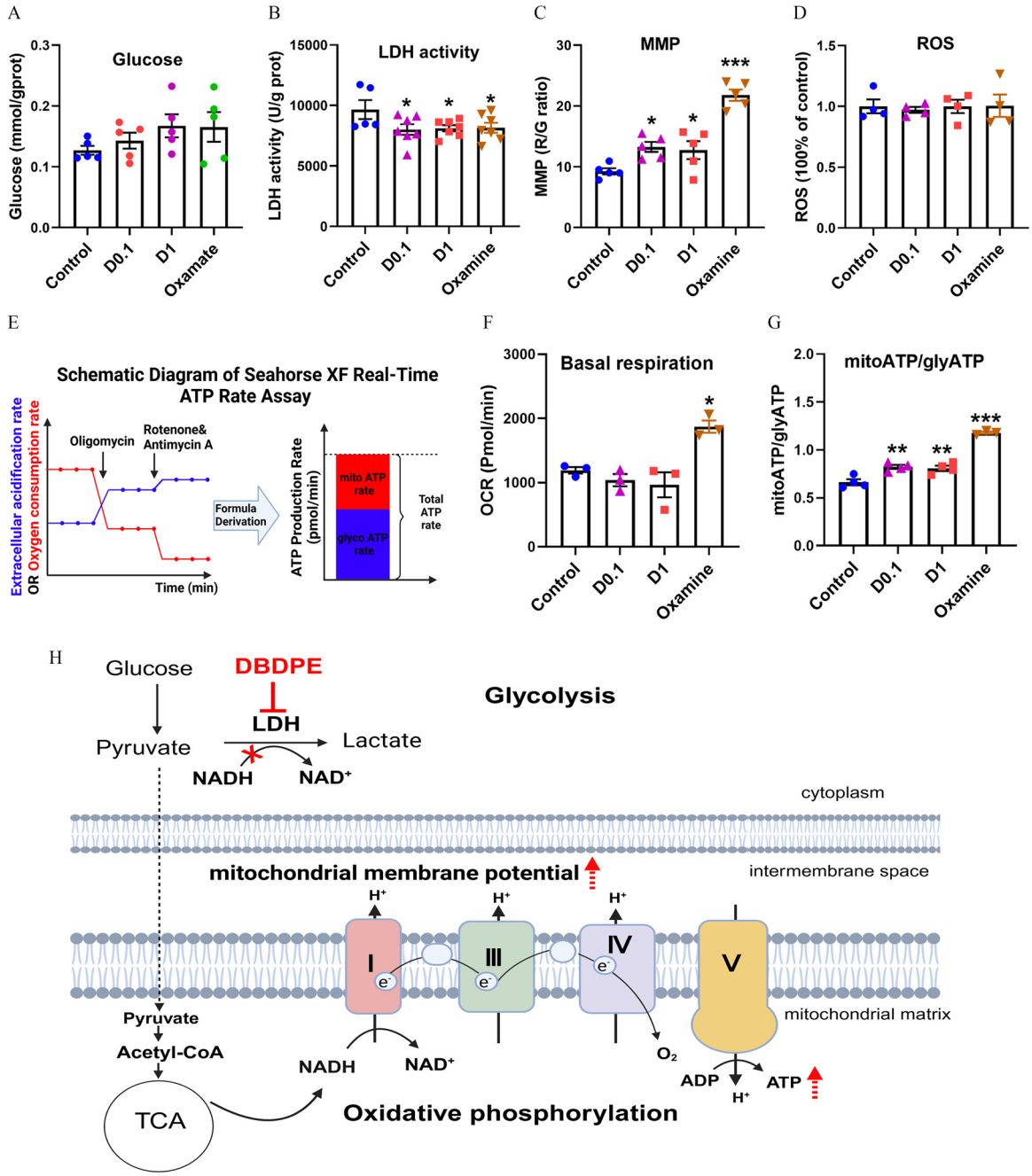

Figure 9. Energy metabolic levels in mouse spermatogonial GC-1 cells exposed to DBDPE and oxamate (LDH inhibitor) *in vitro*. (A) Glucose content in GC-1 cells treated for 72 h ($n = 5$). (B) LDH activity in GC-1 cells treated for 72 h ($n = 5$–7). (C) Mitochondrial membrane potential (MMP) of GC-1 cells treated for 72 h ($n = 5$). (D) ROS levels in GC-1 cells treated for 72 h ($n = 4$). (E) Schematic diagram of the Seahorse XF real-time ATP rate assay. The relative contributions of mitochondrial oxidative phosphorylation and glycolysis to ATP can be determined. The illustration was created in BioRender (2023) https://BioRender.com/p67n031. (F) Quantification of basal respiration in response to DBDPE or oxamate (LDH inhibitor) after 72 h of treatment ($n = 3$). (G) Glycolysis-derived ATP (glycoATP)/mitochondrial oxidative phosphorylation-derived ATP (mitoATP) ratio in GC-1 cells exposed to DBDPE (0.1 μM and 1 μM) and oxamate (LDH inhibitor) for 72 h ($n = 3$–4). Each dot in (A–D,F,G) represents one replicate data point (one well of cells/replicate). (H) Proposed action of DBDPE on glycolysis and oxidative phosphorylation based on findings of the *in vitro* and *in vivo* studies. The illustration was created in BioRender (2023) https://BioRender.com/g29w956. Upward dashed arrows (in red) indicate elevation. The red cross indicates inhibition. Results are represented as means ± standard errors of the mean (SEMs). Data are reported in Excel Table S9. Note: ATP, adenosine triphosphate; D, DBDPE, decabromodiphenyl ethane; G, green; LDH, lactate dehydrogenase; NAD^+, nicotinamide adenine dinucleotide; NADH, nicotinamide adenine dinucleotide reduced; R, red; ROS, reactive oxygen species; TCA, tricarboxylic acid (cycle). $^*p < 0.05$, $^{**}p < 0.01$, and $^{***}p < 0.001$ indicate significant differences between exposure and control groups, by one-way analysis of variance (ANOVA) followed by the post hoc least significant difference (LSD) test.

and the phosphatidylinositol signaling system ($p = 0.041839$, top 7; Excel Table S4) were enriched. The PI3K/Akt signaling pathway is known to regulate cell cycle progression.[73] Consistently, KEGG analysis of proteins harboring differentially phosphorylated sites revealed enrichment of several pathways, including base excision repair, homologous recombination, mismatch repair, and DNA replication, whereas GO analysis of the phosphoproteome highlighted chromosome organization, chromatin organization, and cytoskeleton organization in the 100 nM DBDPE-exposed group. The qRT-PCR analysis in the zebrafish

testes demonstrated that the proposed pathways (e.g., apoptosis and necroptosis, DNA damage and repair, cell cycle, PI3K-AKT pathways) from the proteome and phosphoproteome analysis at the highest concentration were also affected at lower concentrations (0.1, 1, 10 nM). All these enriched pathways are involved in DNA damage responses.[74,75] In fact, DNA damage and apoptosis have been observed in testes of rats following oral administration of DBDPE at 50 or 500 mg/kg per day.[35,36] Similarly, in the present study, DNA damage did occur in the SPD, SPG-I, and SPG-II as characterized by a higher expression of a biomarker (γ-H2AX) for DNA DSBs in testes of zebrafish following exposure to DBDPE at concentrations ≥1 nM. Consistent with our results, oral administration of DBDPE at 50 μg/kg body weight per day to female mice for 30 d also resulted in significantly increased expression of γ-H2AX in both male and female pronuclei (PN) of zygotes obtained by mating the exposed females with sexually matured unexposed males.[76] Together, these results suggest that DBDPE exposure can induce DNA damage. Interestingly, significantly more TUNEL-positive cells were only observed in the testes of zebrafish upon exposure to 100 nM DBDPE. As the most serious form of DNA damage, DSBs have been well established as a common ultimate apoptosis-triggering lesion that arises from primary DNA lesions during DNA replication.[77,78] Thus, we can infer that the testicular outcomes at 100 nM DBDPE exposure may be driven by apoptosis due to DNA damage instead of the direct action of DBDPE. Furthermore, we also observed significantly higher expression levels of cleaved PARP, cleaved caspase-3, and P-JNK-1/2 via Western blotting, supporting apoptosis and DNA damage outcomes in DBDPE-exposed zebrafish testes. Although the apoptosis marker (TUNEL) was not observed to be higher in testes at lower concentrations, the transcription of genes associated with DNA damage responses (e.g., *lig3*, *pold1*, *parp1*, *parp2*, *brca2*, *tp53bpa1*, *jak3*, *akt1s1*, *ripk3*)[75,79,80] and the expression of cleaved caspase-3 and P-JNK-1/2[80] demonstrated an upward trend or significantly higher levels, which suggested a status of DNA damage repair and possible triggering of pre-apoptosis. However, more studies are needed to investigate this hypothesis. Taken together, these results suggest that DNA integrity and stability in testicular germ cells are sensitive to DBDPE exposure, and DNA damage may trigger a series of cell cycle regulation processes associated with DNA damage repair.

Most previous studies have attributed pollutant-induced DNA damage to excessive ROS accumulation accompanied by mitochondrial impairment.[81,82] In our previous study, exposure to DBDPE at 400 μg/L (equal to 412 nM) was found to inhibit the activity of mitochondrial respiratory chain complexes, causing decreased MMP, reduced ATP synthesis, and increased ROS levels in zebrafish embryos/larvae.[34] However, in the present study, we failed to observe significantly different ROS levels in zebrafish testes after exposure to DBDPE. This observation may indicate that the DNA damage (manifested by the increased expression of γ-H2AX) detected in our study was not related to ROS. Nuclear actin polymerization to form filamentous actin (F-actin) plays an important role in the responses to DNA damage and DNA replication stress to maintain genome stability.[83] It has been reported that disruption of F-actin and the subsequent release of DNase I into the nucleus is a novel mechanism that cleaves DNA to generate γ-H2AX in response to chemical exposure.[84] A recent study showed that DBDPE exposure of female mice to 50 μg/kg body weight per day resulted in DNA damage responses (increased expression of γ-H2AX) by affecting the assembly of the nuclear F-actin in the PN of zygotes.[76] Our combined proteome and phosphoproteome analyses showed that key proteins involved in F-actin assembly were significantly less expressed in the DBDPE-exposed fish, which may contribute to the observed DNA damage. However, it is unclear whether this was a direct effect of the DBDPE or related to the cell death identified at this exposure. Although the NAD^+/NADH ratio (an important indicator of the redox state) was lower, MMP was significantly higher, suggesting MHP in testicular cells. The occurrence of MHP is considered a prerequisite for apoptosis, but cells can remain viable under this condition.[85] This may explain the lack of differences in ROS levels in the testes, possibly due to the exposure duration not being sufficient to induce more severe effects. Indeed, a recent study reported that MMP can serve as a sensitive indicator for screening mitochondrial toxicants, can be used for water quality monitoring, and can be used to evaluate a wide range of mitochondrial toxicants covering chemicals with diverse molecular initiating events (MIEs), given that multiple MIEs can be involved in MMP disruption.[86]

However, MMP is not the only determinant of ATP content, especially in spermatogenic cells using lactate as their energy substrate.[41] Significantly lower LDH levels and less activity suggested an impaired capacity to convert pyruvate to lactate, supported by the observed lower lactate/pyruvate ratio and greater accumulation of glucose. Consistently, the PPI network analysis also suggested greater oxidative phosphorylation and less glycolysis. Hence, the greater ATP content could be explained by more efficient ATP production via oxidative phosphorylation. Taken together, the above results suggest possible energy reprogramming by shifting from glycolysis to oxidative phosphorylation in the testes of zebrafish following DBDPE exposure.

Validation of DNA Damage and Energy Metabolism in GC-1 Cells

To further confirm the existence of a dosage window and the occurrence of energy reprogramming upon DBDPE exposure, we conducted an *in vitro* study using the GC-1 spermatogonial cell line. For this purpose, pre–apoptosis-inducing doses (0.1 and 1 μM) were selected based on the altered MMP and ATP profiles. Furthermore, the primary role of LDH inhibition was also verified using oxamate as a positive control for glycolysis inhibition. As expected, cells exposed to 20 mM oxamate or 1 μM DBDPE demonstrated higher levels of γ-H2AX. In addition, the expression levels of proteins associated with DNA damage responses and cell death (PRAP, p-JNK1/2, RIPK3, p-MLKL, and cleaved caspase-3/8) were also significantly higher in both treatments. Except for higher MMP, we also observed significantly lower LDH activity, slightly higher glucose levels, and ROS levels that were not significantly different in GC-1 cells exposed to DBDPE or oxamate compared with control. However, the flow cytometry results showed that the early apoptosis, late apoptosis, and mortality rates of GC-1 cells did not differ significantly from control after exposure to any dose of DBDPE or oxamate. These results indicate that exposure to DBDPE at the selected concentrations was associated with DNA damage, mitochondrial hyperpolarization, and greater cell death signaling but not associated with a higher rate of apoptosis. These results are consistent with those obtained from *in vivo* experiments, thereby providing additional evidence for the existence of a dosage window for DBDPE before inducing germ cell apoptosis. The results may also suggest spermatogonia would be sensitive to direct exposure to environmental chemicals.

To further confirm the occurrence of energy programming, we determined the ATP content generated by the two pathways using Seahorse XF real-time ATP rate assays. A higher mitoATP/glyATP ratio suggested an energy metabolic shift from glycolysis to oxidative phosphorylation in GC-1 cells. We also noted that the

changing profiles of most of the determined parameters showed positive correlations (correlation coefficients ranging from 0.804 to 0.999) between the 1 μM DBDPE-treatment group and the oxamate-treatment group, demonstrating a similar mechanism of action for the two chemicals. Therefore, we speculate that DBDPE may suppress glycolysis by inhibiting LDH activity and enhance oxidative phosphorylation, thereby reprogramming the energy metabolic process in germ cells.

Environmental Implications

In the present study, the lowest concentration (0.1 nM = 97.1 ng/L) of DBDPE for zebrafish exposure was comparable to the highest detected concentration (107 ng/L) in surface water.[15] This means that, at least in some cases, aquatic wild animals may face levels of external exposure risks similar to those of the test subjects in our *in vivo* experiment. Furthermore, the highest reported contents in wild crucian carp (*Carassius auratus*) (1,700 ± 744 ng/g lw)[20] were even higher than those detected in testes from zebrafish after the 2-month DBDPE exposure (870.84 ± 98.45, 1,284.2 ± 482.54, 1,410.83 ± 29.09 ng/g lw in the 0.1, 1, and 10 nM DBDPE-exposure groups) in the present study. One possible explanation could be that wild fish spend their entire life time in water, so they have a longer time window to accumulate waterborne pollutants, leading to higher internal exposure risks. Specifically, exposure to DBDPE for 2 months decreased the TM and PM of zebrafish spermatozoa at all the tested concentrations and inhibited spermatogenesis at the highest concentrations, suggesting impaired functions in the male fish. These findings suggest potential risks for male reproductive toxicity in wild fish experiencing DBDPE exposure, and the multigenerational effects are of particular concern and need further research.

Further research revealed DNA damage both in zebrafish testes and mammalian cells (i.e., GC-1 cells) after exposure to DBDPE. Internal doses of up to 1,590 ng/g lw have been reported in the serum of nonoccupational populations from a BFR-producing area.[22] Despite the lack of exact dose data in testes from humans at present, it can be predicted that humans will be faced with long-term and persistent exposure to DBDPE due to the continued increase in the use and release of DBDPE into the environment. Given the evolutionary conservation of the mechanisms of DSBs (the observed DNA damage type in the present study) formation and repair in different species,[87,88] our results may implicate potential inducing effects of DNA damage in humans and provide theoretical bases for speculating human health effects based on fish and cell experiment results. In addition, the present study also provides an example for establishing NAMs comprising *in vitro*, *ex vivo*, and non-rodent *in vivo* tests for pollutant risk assessment.

Research Limitation

However, certain limitations warrant comment. Notably, the proteomics/phospho-proteomics were limited to the highest concentration of DBDPE in zebrafish testes that exclusively demonstrated overt toxicity, including testicular cell apoptosis, which may not fully represent the effects of environmentally relevant exposure concentrations. Although the qRT-PCR analysis suggested that the proposed pathways at the highest concentration of DBDPE were also affected at lower concentrations, it may not suggest these responses would ultimately result in overt outcomes, such as cell death. Therefore, further research is needed to determine the specific impacts of these biological pathways and their correlation with testicular cell fate. Another limitation is about the difficulty of extrapolating the present results to human health. For one thing, there are many challenges when translating doses used in animal studies to humans, including the dearth of human exposure, toxicokinetic data, and differences in bioavailability for different exposure routes.[89] These challenges underscore the importance of the collection of comprehensive data and information and call for further study. For another, mammalian spermatogenesis is more complex than that of zebrafish, possibly resulting in species-specific responses to DBDPE exposure. Thus, the extrapolation of the present findings to human health also warrants more investigation with optimal models (e.g., mice models).

Conclusions

In conclusion, our results suggest that DBDPE exposure could impair sperm quality and spermatogenesis, and the underlying mechanism could be attributed to DNA damage and energy metabolic reprogramming in testicular germ cells by shifting glycolysis to oxidative phosphorylation. Moreover, MMP could be used as a sensitive indicator of male reproductive impairment, both *in vivo* and *in vitro*. The dosage window characterized by greater MMP in combination with ROS and apoptosis that was not significantly different from controls may provide useful indications for early prediction and intervention of pollutant-induced cellular damage. The integrated *in vitro*, *ex vivo*, and *in vivo* analyses of male reproductive toxicity may provide new methodologies and expedite pollutant risk assessment in future studies.

Acknowledgments

L.Y. and Y.Z. contributed equally to this work. J. Hua, L.Y., and Y.Z. designed the study. J. Han, Y.Z., and G.S. performed *ex vivo* experiments. J. Han, Y.Z., L.Y., T.Z., X.R., and Z.X. performed animal experiments, Y.Z., J. Han, and N.Z. performed *in vitro* experiments. Y.Z., J. Han, and N.Z. performed bioinformatics analysis. Y.Z., L.Y., J. Han, T.Z., and F.L. performed data collection and analysis. J. Hua, L.Y., Y.Z., and B. Zhu provided experimental design guidance and interpretation of results. L.Y. and J.H. wrote the manuscript. L.Y., J. Hua, and B. Zhou edited the manuscript.

We thank Yuan Xiao, Yan Wang, Yuan Sun, Fang Zhou, Guangxin Wang, and Zhenfei Xing from the Analytical and Testing Center of Institute of Hydrobiology, Chinese Academy of Sciences, for their technical support in scanning and transmission electron microscopy (EM) analysis, flow cytometry, Seahorse assay, confocal microscope, and EM sample preparation.

This work was supported by the National Key Research and Development Program of China [grant 2022YFC3902102 (to L.Y.)] and the National Natural Science Foundation of China [grants 22006035 (to J. Hua.), 42377281 (to L.Y.), 42207332 (to B.Z.)].

References

1. Cooper TG, Noonan E, von Eckardstein S, Auger J, Baker HWG, Behre HM, et al. 2010. World Health Organization reference values for human semen characteristics. Hum Reprod Update 16(3):231–245, PMID: 19934213, https://doi.org/10.1093/humupd/dmp048.
2. Pizzol D, Foresta C, Garolla A, Demurtas J, Trott M, Bertoldo A, et al. 2021. Pollutants and sperm quality: a systematic review and meta-analysis. Environ Sci Pollut Res Int 28(4):4095–4103, PMID: 33196997, https://doi.org/10.1007/s11356-020-11589-z.
3. Carlsen E, Giwercman A, Keiding N, Skakkebaek NE. 1992. Evidence for decreasing quality of semen during past 50 years. BMJ 305(6854):609–613, PMID: 1393072, https://doi.org/10.1136/bmj.305.6854.609.
4. Kumar S, Sharma A, Thaker R. 2021. Air pollutants and impairments of male reproductive health—an overview. Rev Environ Health 36(4):565–575, PMID: 33544535, https://doi.org/10.1515/reveh-2020-0136.

5. Albert O, Huang JY, Aleksa K, Hales BF, Goodyer CG, Robaire B, et al. 2018. Exposure to polybrominated diphenyl ethers and phthalates in healthy men living in the greater Montreal area: study of hormonal balance and semen quality. Environ Int 116: 165–175, PMID: 29684825, https://doi.org/10.1016/j.envint.2018.04.012.
6. Yu Y-J, Lin B-G, Liang W-B, Li L-Z, Hong Y-D, Chen X-C, et al. 2018. Associations between PBDEs exposure from house dust and human semen quality at an e-waste areas in South China—a pilot study. Chemosphere 198:266–273, PMID: 29421738, https://doi.org/10.1016/j.chemosphere.2018.01.150.
7. Stieger G, Scheringer M, Ng CA, Hungerbühler K. 2014. Assessing the persistence, bioaccumulation potential and toxicity of brominated flame retardants: data availability and quality for 36 alternative brominated flame retardants. Chemosphere 116:118–123, PMID: 24656972, https://doi.org/10.1016/j.chemosphere.2014.01.083.
8. Zuiderveen EAR, Slootweg JC, de Boer J. 2020. Novel brominated flame retardants—a review of their occurrence in indoor air, dust, consumer goods and food. Chemosphere 255:126816, PMID: 32417508, https://doi.org/10.1016/j.chemosphere.2020.126816.
9. Shen K, Li L, Liu J, Chen C, Liu J. 2019. Stocks, flows and emissions of DBDPE in China and its international distribution through products and waste. Environ Pollut 250:79–86, PMID: 30981938, https://doi.org/10.1016/j.envpol.2019.03.090.
10. Chen Z, Ma T, Liu W, Yuan G, Pan X, Zhang M, et al. 2024. Brominated flame retardants (BFRs) in China over the past half-century: stocks, flows, fates, and ecological risks. Environ Sci Technol 58(31):13613–13623, PMID: 39051121, https://doi.org/10.1021/acs.est.4c00183.
11. An Q, Yang L, Yang S, Wang Y, Shi L, Aamir M, et al. 2023. Legacy and novel brominated flame retardants in agricultural soils of eastern China (2011–2021): concentration level, temporal trend, and health risk assessment. J Hazard Mater 446:130631, PMID: 36586335, https://doi.org/10.1016/j.jhazmat.2022.130631.
12. Liu L, Zhen X, Wang X, Zhang D, Sun L, Tang J. 2021. Spatio-temporal variations and input patterns on the legacy and novel brominated flame retardants (BFRs) in coastal rivers of North China. Environ Pollut 283:117093, PMID: 33857880, https://doi.org/10.1016/j.envpol.2021.117093.
13. Wang N, Lai C, Xu F, Huang D, Zhang M, Zhou X, et al. 2023. A review of polybrominated diphenyl ethers and novel brominated flame retardants in Chinese aquatic environment: source, occurrence, distribution, and ecological risk assessment. Sci Total Environ 904:166180, PMID: 37562617, https://doi.org/10.1016/j.scitotenv.2023.166180.
14. Liu L, Li Y, Zhang J, Niu D, Wang J, Tang J. 2023. Influence of hydrodynamic conditions on the fate of halogenated flame retardants along salinity gradients in a highly polluted micro-tidal estuary. Sci Total Environ 893:164716, PMID: 37301402, https://doi.org/10.1016/j.scitotenv.2023.164716.
15. Zhen X, Tang J, Liu L, Wang X, Li Y, Xie Z. 2018. From headwaters to estuary: distribution and fate of halogenated flame retardants (HFRs) in a river basin near the largest HFR manufacturing base in China. Sci Total Environ 621:1370–1377, PMID: 29054623, https://doi.org/10.1016/j.scitotenv.2017.10.091.
16. Nyholm JR, Grabic R, Arp HPH, Moskeland T, Andersson PL. 2013. Environmental occurrence of emerging and legacy brominated flame retardants near suspected sources in Norway. Sci Total Environ 443:307–314, PMID: 23201697, https://doi.org/10.1016/j.scitotenv.2012.10.081.
17. Zeng Y-H, Luo X-J, Sun Y-X, Yu L-H, Chen S-J, Mai B-X. 2011. [Concentration and emission fluxes of halogenated flame retardants in sewage from sewage outlet in Dongjiang River]. Huan Jing Ke Xue 32(10):2891–2895, PMID: 22279897.
18. Hou R, Lin L, Li H, Liu S, Xu X, Xu Y, et al. 2021. Occurrence, bioaccumulation, fate, and risk assessment of novel brominated flame retardants (NBFRs) in aquatic environments—a critical review. Water Res 198:117168, PMID: 33962238, https://doi.org/10.1016/j.watres.2021.117168.
19. Hou R, Huang Q, Pan Y, Lin L, Liu S, Li H, et al. 2022. Novel brominated flame retardants (NBFRs) in a tropical marine food web from the South China Sea: the influence of hydrophobicity and biotransformation on structure-related trophodynamics. Environ Sci Technol 56(5):3147–3158, PMID: 35175039, https://doi.org/10.1021/acs.est.1c08104.
20. Tao L, Zhang Y, Wu J-P, Wu S-K, Liu Y, Zeng Y-H, et al. 2019. Biomagnification of PBDEs and alternative brominated flame retardants in a predatory fish: using fatty acid signature as a primer. Environ Int 127:226–232, PMID: 30928846, https://doi.org/10.1016/j.envint.2019.03.036.
21. Chen T, Yu D, Yang L, Sui S, Lv S, Bai Y, et al. 2019. Thyroid function and decabromodiphenyl ethane (DBDPE) exposure in Chinese adults from a DBDPE manufacturing area. Environ Int 133(pt A):105179, PMID: 31627134, https://doi.org/10.1016/j.envint.2019.105179.
22. Zhao X, Chen T, Yang B, Wang D, Sun W, Wang Y, et al. 2021. Serum levels of novel brominated flame retardants (NBFRs) in residents of a major BFR-producing region: occurrence, impact factors and the relationship to thyroid and liver function. Ecotoxicol Environ Saf 208:111467, PMID: 33080422, https://doi.org/10.1016/j.ecoenv.2020.111467.
23. Shi Z, Zhang L, Li J, Zhao Y, Sun Z, Zhou X, et al. 2016. Novel brominated flame retardants in food composites and human milk from the Chinese Total Diet Study in 2011: concentrations and a dietary exposure assessment. Environ Int 96:82–90, PMID: 27619751, https://doi.org/10.1016/j.envint.2016.09.005.
24. Qiao L, Zheng X-B, Yan X, Wang M-H, Zheng J, Chen S-J, et al. 2018. Brominated flame retardant (BFRs) and dechlorane plus (DP) in paired human serum and segmented hair. Ecotoxicol Environ Saf 147:803–808, PMID: 28954370, https://doi.org/10.1016/j.ecoenv.2017.09.047.
25. Chen T, Huang M, Li J, Li J, Shi Z. 2019. Polybrominated diphenyl ethers and novel brominated flame retardants in human milk from the general population in Beijing, China: occurrence, temporal trends, nursing infants' exposure and risk assessment. Sci Total Environ 689:278–286, PMID: 31276995, https://doi.org/10.1016/j.scitotenv.2019.06.442.
26. Sala B, Garcia-Garin O, Borrell A, Aguilar A, Víkingsson GA, Eljarrat E. 2022. Transplacental transfer of plasticizers and flame retardants in fin whales (*Balaenoptera physalus*) from the North Atlantic Ocean. Environ Pollut 313:120168, PMID: 36115483, https://doi.org/10.1016/j.envpol.2022.120168.
27. Barón E, Giménez J, Verborgh P, Gauffier P, De Stephanis R, Eljarrat E, et al. 2015. Bioaccumulation and biomagnification of classical flame retardants, related halogenated natural compounds and alternative flame retardants in three delphinids from Southern European waters. Environ Pollut 203:107–115, PMID: 25875161, https://doi.org/10.1016/j.envpol.2015.03.041.
28. Aznar-Alemany Ò, Sala B, Jobst KJ, Reiner EJ, Borrell A, Aguilar À, et al. 2021. Temporal trends of halogenated and organophosphate contaminants in striped dolphins from the Mediterranean Sea. Sci Total Environ 753:142205, PMID: 33207472, https://doi.org/10.1016/j.scitotenv.2020.142205.
29. Wang Y, Yang Y, Dang C, Lu B, Luo Y, Fu J. 2023. Is it really safe to replace decabromodiphenyl ether (BDE209) with decabromodiphenyl ethane (DBDPE)? A perspective from hepatotoxicity. Environ Toxicol 38(4):844–856, PMID: 36660779, https://doi.org/10.1002/tox.23727.
30. Dong L, Wang S, Zhang L, Liu D, You H. 2023. DBDPE and ZnO NPs synergistically induce neurotoxicity of SK-N-SH cells and activate mitochondrial apoptosis signaling pathway and Nrf2-mediated antioxidant pathway. J Hazard Mater 441:129872, PMID: 36084461, https://doi.org/10.1016/j.jhazmat.2022.129872.
31. Wang C, Zeng L, Li Y, Shi C, Peng Y, Pan R, et al. 2022. Decabromodiphenyl ethane induces locomotion neurotoxicity and potential Alzheimer's disease risks through intensifying amyloid-beta deposition by inhibiting transthyretin/transthyretin-like proteins. Environ Int 168:107482, PMID: 35998411, https://doi.org/10.1016/j.envint.2022.107482.
32. Wang X, Ling S, Guan K, Luo X, Chen L, Han J, et al. 2019. Bioconcentration, biotransformation, and thyroid endocrine disruption of decabromodiphenyl ethane (DBDPE), a novel brominated flame retardant, in zebrafish larvae. Environ Sci Technol 53(14):8437–8446, PMID: 31188578, https://doi.org/10.1021/acs.est.9b02831.
33. Wang Y, Wang X, Sui S, Liu Z. 2023. Endocrine disrupting and carcinogenic effects of decabromodiphenyl ether. Front Endocrinol (Lausanne) 14:1183815, PMID: 37334308, https://doi.org/10.3389/fendo.2023.1183815.
34. Sun Y, Xu Y, Wu H, Hou J. 2024. A critical review on BDE-209: source, distribution, influencing factors, toxicity, and degradation. Environ Int 183:108410, PMID: 38160509, https://doi.org/10.1016/j.envint.2023.108410.
35. Li X, Liu J, Zhou G, Sang Y, Zhang Y, Jing L, et al. 2021. BDE-209 and DBDPE induce male reproductive toxicity through telomere-related cell senescence and apoptosis in SD rat. Environ Int 146:106307, PMID: 33395949, https://doi.org/10.1016/j.envint.2020.106307.
36. Xue J, Li X, Liu J, Zhang Y, Sang Y, Zhou G, et al. 2022. Decabromodiphenyl ethane induces male reproductive toxicity by glycolipid metabolism imbalance and meiotic failure. Ecotoxicol Environ Saf 246:114165, PMID: 36228355, https://doi.org/10.1016/j.ecoenv.2022.114165.
37. Sun RB, Shang S, Zhang W, Lin BC, Wang Q, Shi Y, et al. 2018. Endocrine disruption activity of 30-day dietary exposure to decabromodiphenyl ethane in Balb/C mouse. Biomed Environ Sci 31(1):12–22, PMID: 29409581, https://doi.org/10.3967/bes2018.002.
38. Yang L, Zhu B, Zhou S, Zhao M, Li R, Zhou Y, et al. 2023. Mitochondrial dysfunction was involved in decabromodiphenyl ethane-induced glucolipid metabolism disorders and neurotoxicity in zebrafish larvae. Environ Sci Technol 57(30):11043–11055, PMID: 37467077, https://doi.org/10.1021/acs.est.3c03552.
39. Braeuning A, Balaguer P, Bourguet W, Carreras-Puigvert J, Feiertag K, Kamstra JH, et al. 2023. Development of new approach methods for the identification and characterization of endocrine metabolic disruptors—a PARC project. Front Toxicol 5:1212509, PMID: 37456981, https://doi.org/10.3389/ftox.2023.1212509.
40. Heindel JJ, Blumberg B, Cave M, Machtinger R, Mantovani A, Mendez MA, et al. 2017. Metabolism disrupting chemicals and metabolic disorders. Reprod Toxicol 68:3–33, PMID: 27760374, https://doi.org/10.1016/j.reprotox.2016.10.001.
41. Boussouar F, Benahmed M. 2004. Lactate and energy metabolism in male germ cells. Trends Endocrinol Metab 15(7):345–350, PMID: 15350607, https://doi.org/10.1016/j.tem.2004.07.003.

42. Vaupel P, Schmidberger H, Mayer A. 2019. The Warburg effect: essential part of metabolic reprogramming and central contributor to cancer progression. Int J Radiat Biol 95(7):912–919, PMID: 30822194, https://doi.org/10.1080/09553002.2019.1589653.
43. Aurrière J, Goudenège D, Baris OR, Boguenet M, May-Panloup P, Lenaers G, et al. 2021. Cancer/testis antigens into mitochondria: a hub between spermatogenesis, tumorigenesis and mitochondrial physiology adaptation. Mitochondrion 56:73–81, PMID: 33220498, https://doi.org/10.1016/j.mito.2020.11.002.
44. Jiang X, Shi P, Jiang L, Qiu J, Xu B, Pan Y, et al. 2022. *In vivo* toxicity evaluations of halophenolic disinfection byproducts in drinking water: a multi-omics analysis of toxic mechanisms. Water Res 218:118431, PMID: 35468502, https://doi.org/10.1016/j.watres.2022.118431.
45. Sun J, Tang S, Peng H, Saunders DMV, Doering JA, Hecker M, et al. 2016. Combined transcriptomic and proteomic approach to identify toxicity pathways in early life stages of Japanese medaka (*Oryzias latipes*) exposed to 1,2,5,6-tetrabromocyclooctane (TBCO). Environ Sci Technol 50(14):7781–7790, PMID: 27322799, https://doi.org/10.1021/acs.est.6b01249.
46. Żarski D, Horváth Á, Bernáth G, Palińska-Żarska K, Krejszeff S, Müller T, et al. 2014. Application of different activating solutions to in vitro fertilization of crucian carp, *Carassius carassius* (L.), eggs. Aquacult Int 22(1):173–184, https://doi.org/10.1007/s10499-013-9692-z.
47. Shaliutina O, Materiienko A, Shaliutina-Kolešová A, Gazo I. 2021. Using fish spermatozoa in *in vitro* toxicity tests: a potential toxicology tool. Aquaculture 539:736647, https://doi.org/10.1016/j.aquaculture.2021.736647.
48. Kollár T, Kása E, Ferincz Á, Urbányi B, Csenki-Bakos Z, Horváth Á. 2018. Development of an in vitro toxicological test system based on zebrafish (*Danio rerio*) sperm analysis. Environ Sci Pollut Res Int 25(15):14426–14436, PMID: 29525864, https://doi.org/10.1007/s11356-018-1613-2.
49. Hatef A, Alavi SMH, Golshan M, Linhart O. 2013. Toxicity of environmental contaminants to fish spermatozoa function *in vitro*—a review. Aquat Toxicol 140–141:134–144, PMID: 23792626, https://doi.org/10.1016/j.aquatox.2013.05.016.
50. Nordgreen J, Tahamtani FM, Janczak AM, Horsberg TE. 2014. Behavioural effects of the commonly used fish anaesthetic tricaine methanesulfonate (MS-222) on zebrafish (*Danio rerio*) and its relevance for the acetic acid pain test. PLoS One 9(3):e92116, PMID: 24658262, https://doi.org/10.1371/journal.pone.0092116.
51. Matthews JL, Murphy JM, Carmichael C, Yang H, Tiersch T, Westerfield M, et al. 2018. Changes to extender, cryoprotective medium, and *in vitro* fertilization improve zebrafish sperm cryopreservation. Zebrafish 15(3):279–290, PMID: 29369744, https://doi.org/10.1089/zeb.2017.1521.
52. OECD (Organisation for Economic Co-operation and Development). 2013. *Test No. 236: Fish Embryo Acute Toxicity (FET) test, OECD Guidelines for the Testing of Chemicals, Section 2.* Paris, France: OECD Publishing. https://doi.org/10.1787/9789264203709-en.
53. Zhang S-Y, Gan X, Shen B, Jiang J, Shen H, Lei Y, et al. 2023. 6PPD and its metabolite 6PPDQ induce different developmental toxicities and phenotypes in embryonic zebrafish. J Hazard Mater 455:131601, PMID: 37182464, https://doi.org/10.1016/j.jhazmat.2023.131601.
54. Notarangelo G, Spinelli JB, Perez EM, Baker GJ, Kurmi K, Elia I, et al. 2022. Oncometabolite d-2HG alters T cell metabolism to impair $CD8^+$ T cell function. Science 377(6614):1519–1529, PMID: 36173860, https://doi.org/10.1126/science.abj5104.
55. Hong X, Chen R, Zhang L, Yan L, Li J, Zha J. 2022. Low doses and lifecycle exposure of waterborne antidepressants in zebrafish model: a survey on sperm traits, reproductive behaviours, and transcriptome responses. Sci Total Environ 832:155017, PMID: 35395305, https://doi.org/10.1016/j.scitotenv.2022.155017.
56. Sáez-Espinosa P, Franco-Esclapez C, Robles-Gómez L, Silva WTAF, Romero A, Immler S, et al. 2022. Morphological and ultrastructural alterations of zebrafish (*Danio rerio*) spermatozoa after motility activation. Theriogenology 188:108–115, PMID: 35688040, https://doi.org/10.1016/j.theriogenology.2022.05.025.
57. Wiśniewski JR, Zougman A, Nagaraj N, Mann M. 2009. Universal sample preparation method for proteome analysis. Nat Methods 6(5):359–362, PMID: 19377485, https://doi.org/10.1038/nmeth.1322.
58. Schneider CA, Rasband WS, Eliceiri KW. 2012. NIH image to ImageJ: 25 years of image analysis. Nat Methods 9(7):671–675, PMID: 22930834, https://doi.org/10.1038/nmeth.2089.
59. Xie H, Wang X, Jin M, Li L, Zhu J, Kang Y, et al. 2022. Cilia regulate meiotic recombination in zebrafish. J Mol Cell Biol 14(7):mjac049, PMID: 35981808, https://doi.org/10.1093/jmcb/mjac049.
60. Xiong P, Yan X, Zhu Q, Qu G, Shi J, Liao C, et al. 2019. A review of environmental occurrence, fate, and toxicity of novel brominated flame retardants. Environ Sci Technol 53(23):13551–13569, PMID: 31682424, https://doi.org/10.1021/acs.est.9b03159.
61. Liu M, Li A, Meng L, Zhang G, Guan X, Zhu J, et al. 2022. Exposure to novel brominated flame retardants and organophosphate esters and associations with thyroid cancer risk: a case–control study in eastern China. Environ Sci Technol 56(24):17825–17835, PMID: 36468700, https://doi.org/10.1021/acs.est.2c04759.
62. Egloff C, Crump D, Chiu S, Manning G, McLaren KK, Cassone CG, et al. 2011. *In vitro* and *in ovo* effects of four brominated flame retardants on toxicity and hepatic mRNA expression in chicken embryos. Toxicol Lett 207(1):25–33, PMID: 21893176, https://doi.org/10.1016/j.toxlet.2011.08.015.
63. Zheng X-B, Luo X-J, Zeng Y-H, Wu J-P, Chen S-J, Mai B-X. 2014. Halogenated flame retardants during egg formation and chicken embryo development: maternal transfer, possible biotransformation, and tissue distribution. Environ Toxicol Chem 33(8):1712–1719, PMID: 24888473, https://doi.org/10.1002/etc.2588.
64. Fernie KJ, Chabot D, Champoux L, Brimble S, Alaee M, Marteinson S, et al. 2017. Spatiotemporal patterns and relationships among the diet, biochemistry, and exposure to flame retardants in an apex avian predator, the peregrine falcon. Environ Res 158:43–53, PMID: 28599194, https://doi.org/10.1016/j.envres.2017.05.035.
65. Ozgur ME, Ulu A, Balcioglu S, Ozcan I, Okumus F, Koytepe S, et al. 2018. Investigation of toxicity properties of flower-like ZnO nanoparticles on *Cyprinus carpio* sperm cells using computer-assisted sperm analysis (CASA). Turk J Fish Aquat Sci 18:771–780, https://doi.org/10.4194/1303-2712-v18_6_03.
66. Alavi SMH, Hatef A, Pšenička M, Kašpar V, Boryshpolets S, Dzyuba B, et al. 2012. Sperm biology and control of reproduction in sturgeon: (II) sperm morphology, acrosome reaction, motility and cryopreservation. Rev Fish Biol Fish 22(4):861–886, https://doi.org/10.1007/s11160-012-9270-x.
67. Dietrich GJ, Dietrich M, Kowalski RK, Dobosz S, Karol H, Demianowicz W, et al. 2010. Exposure of rainbow trout milt to mercury and cadmium alters sperm motility parameters and reproductive success. Aquat Toxicol 97(4):277–284, PMID: 20044150, https://doi.org/10.1016/j.aquatox.2009.12.010.
68. Han XB, Yuen KWY, Wu RSS. 2013. Polybrominated diphenyl ethers affect the reproduction and development, and alter the sex ratio of zebrafish (*Danio rerio*). Environ Pollut 182:120–126, PMID: 23906559, https://doi.org/10.1016/j.envpol.2013.06.045.
69. He J, Yang D, Wang C, Liu W, Liao J, Xu T, et al. 2011. Chronic zebrafish low dose decabrominated diphenyl ether (BDE-209) exposure affected parental gonad development and locomotion in F1 offspring. Ecotoxicology 20(8):1813–1822, PMID: 21695510, https://doi.org/10.1007/s10646-011-0720-3.
70. Huang Y, Zhu G, Peng L, Ni W, Wang X, Zhang J, et al. 2015. Effect of 2,2′,4,4′-tetrabromodiphenyl ether (BDE-47) on sexual behaviors and reproductive function in male zebrafish (*Danio rerio*). Ecotoxicol Environ Saf 111:102–108, PMID: 25450921, https://doi.org/10.1016/j.ecoenv.2014.09.037.
71. Vested A, Giwercman A, Bonde JP, Toft G. 2014. Persistent organic pollutants and male reproductive health. Asian J Androl 16(1):71–80, PMID: 24369135, https://doi.org/10.4103/1008-682X.122345.
72. Brokken LJS, Lundberg PJ, Spanò M, Manicardi GC, Pedersen HS, Struciński P, et al. 2014. Interactions between polymorphisms in the aryl hydrocarbon receptor signalling pathway and exposure to persistent organochlorine pollutants affect human semen quality. Reprod Toxicol 49:65–73, PMID: 25084496, https://doi.org/10.1016/j.reprotox.2014.07.073.
73. Liang J, Slingerland JM. 2003. Multiple roles of the PI3K/PKB (Akt) pathway in cell cycle progression. Cell Cycle 2(4):339–345, PMID: 12851486, https://doi.org/10.4161/cc.2.4.433.
74. Stanic M, Mekhail K. 2022. Integration of DNA damage responses with dynamic spatial genome organization. Trends Genet 38(3):290–304, PMID: 34598804, https://doi.org/10.1016/j.tig.2021.08.016.
75. Chatterjee N, Walker GC. 2017. Mechanisms of DNA damage, repair, and mutagenesis. Environ Mol Mutagen 58(5):235–263, PMID: 28485537, https://doi.org/10.1002/em.22087.
76. Shi F, Xu Y, Zhang S, Fu Z, Yu Q, Zhang S, et al. 2022. Decabromodiphenyl ethane affects embryonic development by interfering with nuclear F-actin in zygotes and leads to cognitive and social disorders in offspring mice. FASEB J 36(8):e22445, PMID: 35816173, https://doi.org/10.1096/fj.202200586R.
77. Kaina B. 2003. DNA damage-triggered apoptosis: critical role of DNA repair, double-strand breaks, cell proliferation and signaling. Biochem Pharmacol 66(8):1547–1554, PMID: 14555233, https://doi.org/10.1016/s0006-2952(03)00510-0.
78. Lorda-Diez CI, Solis-Mancilla ME, Sanchez-Fernandez C, Garcia-Porrero JA, Hurle JM, Montero JA. 2019. Cell senescence, apoptosis and DNA damage cooperate in the remodeling processes accounting for heart morphogenesis. J Anat 234(6):815–829, PMID: 30875434, https://doi.org/10.1111/joa.12972.
79. Yoshida K, Miki Y. 2004. Role of BRCA1 and BRCA2 as regulators of DNA repair, transcription, and cell cycle in response to DNA damage. Cancer Sci 95(11):866–871, PMID: 15546503, https://doi.org/10.1111/j.1349-7006.2004.tb02195.x.
80. Roos WP, Kaina B. 2006. DNA damage-induced cell death by apoptosis. Trends Mol Med 12(9):440–450, PMID: 16899408, https://doi.org/10.1016/j.molmed.2006.07.007.
81. Shaliutina O, Shaliutina-Kolešová A, Lebeda I, Rodina M, Gazo I. 2017. The *in vitro* effect of nonylphenol, propranolol, and diethylstilbestrol on quality parameters and oxidative stress in sterlet (*Acipenser ruthenus*) spermatozoa. Toxicol In Vitro 43:9–15, PMID: 28533019, https://doi.org/10.1016/j.tiv.2017.05.006.

82. Zhang J, Liu JH, Ren LH, Wei JL, Duan JC, Zhang LF, et al. 2018. $PM_{2.5}$ induces male reproductive toxicity via mitochondrial dysfunction, DNA damage and RIPK1 mediated apoptotic signaling pathway. Sci Total Environ 634:1435–1444, PMID: 29710643, https://doi.org/10.1016/j.scitotenv.2018.03.383.
83. Wollscheid H-P, Ulrich HD. 2023. Chromatin meets the cytoskeleton: the importance of nuclear actin dynamics and associated motors for genome stability. DNA Repair (Amst) 131:103571, PMID: 37738698, https://doi.org/10.1016/j.dnarep.2023.103571.
84. Zhao X, Yang G, Toyooka T, Ibuki Y. 2015. New mechanism of γ-H2AX generation: surfactant-induced actin disruption causes deoxyribonuclease I translocation to the nucleus and forms DNA double-strand breaks. Mutat Res Genet Toxicol Environ Mutagen 794:1–7, PMID: 26653977, https://doi.org/10.1016/j.mrgentox.2015.09.006.
85. Iijima T. 2006. Mitochondrial membrane potential and ischemic neuronal death. Neurosci Res 55(3):234–243, PMID: 16716421, https://doi.org/10.1016/j.neures.2006.04.005.
86. Lee J, König M, Braun G, Escher BI. 2024. Water quality monitoring with the multiplexed assay MitoOxTox for mitochondrial toxicity, oxidative stress response, and cytotoxicity in AREc32 cells. Environ Sci Technol 58(13):5716–5726, PMID: 38503264, https://doi.org/10.1021/acs.est.3c09844.
87. Kawale AS, Sung P. 2020. Mechanism and significance of chromosome damage repair by homologous recombination. Essays Biochem 64(5):779–790, PMID: 32756864, https://doi.org/10.1042/EBC20190093.
88. Li Y, Wu Y-F, Jiang H-W, Khan R, Han Q-Q, Iqbal F, et al. 2021. The molecular control of meiotic double-strand break (DSB) formation and its significance in human infertility. Asian J Androl 23(6):555–561, PMID: 33586697, https://doi.org/10.4103/aja.aja_5_21.
89. Panlilio JM, Aluru N, Hahn ME. 2020. Developmental neurotoxicity of the harmful algal bloom toxin domoic acid: cellular and molecular mechanisms underlying altered behavior in the zebrafish model. Environ Health Perspect 128(11):117002, PMID: 33147070, https://doi.org/10.1289/EHP6652.